Extraembryonic endoderm cells induce neuroepithelial tissue in gastruloids

Noémie M. L. P. Bérenger-Currias[1,2], Maria Mircea*[1], Esmée Adegeest*[1], Patrick R. van den Berg[1], Marleen Feliksik[1], Mazène Hochane[#,1], Timon Idema[#,2], Sander J. Tans[#,2,3], Stefan Semrau[#,1]

* equal contribution
# co-corresponding authors
1. Leiden University, Einsteinweg 55, 2333 CC Leiden, Netherlands
2. Delft University of Technology, Department of Bionanoscience, Kavli Institute of Nanoscience, Van der Maasweg 9, 2629 HZ Delft, Netherlands
3. AMOLF, Science Park 104, 1098 XG Amsterdam, Netherlands

SUMMARY

Stem-cell derived *in vitro* systems, such as organoids or embryoids, hold great potential for modeling *in vivo* biology and engineering living systems with novel functions. To unlock that potential, we need new ways to elicit higher-level organization. Here we show that adding extraembryonic endoderm (XEN) cells to mouse gastruloids leads to the formation of neural epithelia. By single-cell RNA-seq, imaging and differentiation experiments, we demonstrate the neural characteristics and spatial patterning of the epithelial tissue. We further show that the XEN cells differentiate reciprocally to a visceral endoderm-like state. Finally, we demonstrate that local inhibition of WNT signaling and production of a basement membrane by the XEN cells underlie the formation of the neuroepithelial tissue. In summary, we establish "XEN Enhanced Gastruloids" (XEGs) to explore heterotypic cellular interactions as a means to achieve complex, tissue-level organization *in vitro*.

Introduction

Multicellular *in vitro* systems have become a major focus of biology and bioengineering over the last few years. Stem cell-derived systems, such as embryoids and organoids show complex organization and have the potential to exhibit functions that emerge from the interaction of multiple tissues[1-3]. These systems leverage differentiation mechanisms inherent to stem cells and rely heavily on self-organization. Their formation is therefore typically variable and difficult to control. By contrast, defined assemblies of differentiated cell types are much more controllable and can thus be engineered to exhibit novel functions[4], but they are limited in complexity. To exploit the potential of stem cell-derived systems and eventually engineer them, we need to improve our control of these systems.

A promising starting point for complex, engineered systems are gastruloids. These aggregates of mouse or human embryonic stem cells (ESCs) recapitulate elements of embryonic development, such as embryo elongation and body axis formation[5-10]. Recently, tissue-level organization has been achieved by exogenous induction of relevant signaling pathways[11-13]. The possibility to induce various tissues in a controlled and reproducible way, would make gastruloids the ideal template for creating more complex systems.

Thus far, gastruloids are made exclusively from ESCs. *In vivo*, mammalian embryos receive important patterning inputs from extraembryonic cells, especially during the earliest embryonic stages[14]. Extraembryonic endoderm (XEN) cells have therefore been incorporated in embryoid systems[11,15-17]. Remarkably, gastruloids achieve symmetry breaking without external cues from extraembryonic cells. This does not exclude, however, that XEN cells can unlock additional developmental potential and provide an opportunity to control gastruloid organization. XEN cells are derived from the primitive endoderm (PrE), which overlays the developing epiblast (see Fig. 1a for a schematic of early mouse development.) Subsequently,

39 the PrE gives rise to the Parietal Endoderm (PE), which covers the inside of the blastocoel
40 cavity[18] and the Visceral Endoderm (VE), which surrounds the embryo until the formation of
41 the visceral yolk sac and its integration in the embryonic gut[19,20]. A subpopulation of the VE,
42 the Anterior Visceral Endoderm (AVE) has a role in the establishment of the embryo's body
43 axes[21,22]. Hence, XEN cells might have unexplored potential to pattern stem cell-derived model
44 systems.

45 Here we report that aggregates of mouse embryonic stem cells (mESCs) and XEN cells
46 can produce columnar neural epithelia. Using multiple markers, perturbation of the signaling
47 pathways that play a role in neural development *in vivo*, and further differentiation to neural
48 cell types, we confirmed that the epithelial structures indeed have neural characteristics. By
49 single-cell RNA-seq, we identified differences in composition and molecular profiles between
50 our new model system and regular gastruloids. We then established, that XEN-derived cells
51 become visceral endoderm-like due to co-differentiation with the mESCs. Finally, we showed
52 that XEN cells promote epithelia formation by local inhibition of primitive streak formation,
53 likely via the WNT inhibitor DKK1, as well as through production of a basement membrane.
54 Our study thus highlights the complex interplay between embryonic and extraembryonic cells
55 and explores possible mechanisms underlying the great morphogenic potential of stem cell-
56 derived systems
57

58 # Results

59 **XEN cells induce neuroepithelial structures in XEN enhanced gastruloids**

60 We first implemented the original mouse gastruloid protocol[5], in which mESCs are aggregated
61 in N2B27 media and exposed to a pulse of WNT signaling for 24 h. After 96 h, this protocol
62 results in elongated gastruloids. As reported before[5-7], 96 h gastruloids contained localized

63 primitive streak-like and neural progenitor-like compartments, marked by Brachyury (T) and
64 SOX2, respectively (Fig. 1c, inset). Starting from the gastruloid protocol, we developed a new
65 system by aggregating mESCs and XEN cells, keeping all other experimental conditions the
66 same (Fig. 1b). We call our mixed aggregates "XEN Enhanced Gastruloids" (XEGs). Like
67 gastruloids, 96 h XEGs showed an elongated morphology and localized T-positive and SOX2-
68 positive compartments. However, unlike in gastruloids, SOX2+ cells in XEGs were organized
69 in columnar epithelia surrounding one or several lumina (Fig 1c).

70 Expression of the broadly expressed neural marker SOX2 and the striking morphology
71 suggested that the observed structures resemble neural epithelia. The lack of pluripotency
72 marker expression (Supplementary Fig. 1a) excluded that the structures were formed by
73 remaining undifferentiated cells. The presence of N-cadherin and absence of E-cadherin in the
74 epithelia (Fig. 1d, top) is consistent with the known switch from E- to N-cadherin during neural
75 differentiation *in vivo*[23] and *in vitro*[24]. We could also observe that the epithelial cells were
76 polarized and expressed apical markers ZO-1 and aPKC (Fig. 1d, bottom), consistent with
77 neural epithelia *in vivo*[25]. Finally, we detected the neural progenitor markers PAX6 and
78 NKX6.1[26] in a subpopulation of epithelial cells (Supplementary Fig. 1b). Combined, these
79 results suggest that the observed structures in XEGs have the characteristics of neural epithelia.

80 To understand how these structures formed, we used time-lapse microscopy of
81 developing XEGs. Around 48 h after seeding, cells formed rosette-like shapes (Supplementary
82 Fig. 1c), which resembled structures found in Matrigel-embedded mESCs[27,28] and indicated a
83 mesenchymal-epithelial transition. Subsequently, a columnar epithelium was formed. Then
84 lumina opened at different places and merged between 48 h and 72 h (Supplementary Fig. 1d).
85 During the final 24 h, the epithelium kept extending and differentiated further, as revealed by
86 the expression of the neural progenitor marker SOX1[29] (Fig. 1e, bottom). A SOX1 positive cell

87 population also appeared in gastruloids within the same time frame, but, importantly, remained
88 unorganized (Fig. 1e, top).
89 To explore the robustness of the protocol and identify optimal conditions for the
90 formation of epithelial structures, we tested different ratios of mESCs and XEN cells
91 (Supplementary Fig. 1e, f). Interestingly, even the smallest proportion of XEN cells tested
92 (1:5), was able to induce some epithelia formation. On the other hand, elongation and
93 symmetry breaking were inhibited when the proportion of XEN cells exceeded 1:2. A ratio of
94 1:3 gave optimal results, with the concurrence of SOX2-positive epithelia and T-positive cells
95 in nearly all aggregates.
96
97 **Epithelia in XEGs show partial anteroposterior and dorsoventral patterning**
98 To establish, how closely XEGs mimic *in vivo* development, we looked for patterning related
99 to body axis formation. Like in gastruloids, expression of T (Fig. 1c), revealed a posterior-like
100 compartment. Localized expression of anterior markers (ASCL1, PAX6, see Fig. 2a and
101 Supplementary Fig. 1b) indicated an anterior-like compartment, although important canonical
102 markers of the most anterior part of the embryo (OTX2, LEFTY1, EN1, ZIC1) could not be
103 detected in XEGs (data not shown). The presence of anteroposterior patterning was supported
104 by the expression of *Wnt4*, *Wnt8a* and *Fgf8* as gradients along the long axis of XEGs (Fig. 2b),
105 which resembles the pattern found *in vivo*[30]. Neural epithelia in XEGs also expressed markers
106 of both the dorsal (PAX6, MSX1) and ventral (NKX6.1, NRCAM) neural tube (Fig. 2c). While
107 PAX6 and MSX1 were found in cells close to the outside of the XEG (which are usually in
108 contact with the XEN cells), NKX6.1 and NRCAM were expressed broadly throughout the
109 epithelial structures. In summary, 96 h XEGs show indications of anteroposterior and
110 dorsoventral symmetry breaking.
111

112 **Signaling perturbation experiments and further differentiation support the**
113 **neuroepithelial character**

114 To further characterize the neuroepithelial structures, we tested how they respond to signaling
115 inputs found *in vivo*. Specifically, we explored the response to BMP pathway inhibition, as
116 well as Sonic Hedgehog (Shh) and retinoic acid (RA) pathway activation (Fig. 3a, b). The
117 inhibition of BMP signaling, known to prevent premature neural specification[31], resulted in an
118 increased number of neural progenitor-like cells (marked by SOX2, PAX6 and NKX6.1). Sonic
119 hedgehog, produced *in vivo* by the notochord and the floor plate (see schematic in Fig. 3a), is
120 known to be necessary for the patterning of the ventral part of the neural tube[32]. The activation
121 of the Hh signaling pathway led to a higher frequency of cells expressing a ventral marker
122 (NKX6.1) in XEGs. RA, involved in anterior-posterior patterning[33], strongly increased the
123 number of cells expressing PAX6, which is found specifically in the anterior part of the neural
124 tube[34]. The neuroepithelial structures in XEGs thus responded to signaling inputs as expected
125 from *in vivo* development.

126 Even in the absence of RA, some hindbrain markers (ASCL1, PAX6) were sporadically
127 expressed, typically concentrated at one pole of the XEG (Supplementary Fig. 1b, Fig. 2a).
128 This hint of anterior specialization suggested a potential to differentiate further into cerebral
129 tissue. Indeed, within four days of additional culture in cerebral organoid differentiation
130 media[35], XEGs developed a layered organization of neural progenitors (SOX2+/PAX6+) and
131 neurons (TUJ1+/CTIP2+), surrounding cavities, reminiscent of tissue organization around
132 brain ventricles (Fig. 3c, Supplementary Fig. 2a, b). Interestingly, we also observed a
133 population of cells expressing the endothelial marker CD31 (Supplementary Fig. 2c). This
134 might indicate that non-neural cells remained and might have differentiated further. Those
135 CD31+ cells could specifically represent an early stage of vasculature.

136

137 **Single-cell RNA-seq reveals the transcriptional profiles of XEG cells**

138 Having focused on the most striking, morphological difference between gastruloids and XEGs,
139 we wanted to take a more comprehensive approach to reveal additional differences between
140 the two model systems. To that end, we used single-cell RNA-sequencing (scRNA-seq)
141 (Supplementary Fig. 3a-e). By mapping the data to single-cell transcriptomes of mouse
142 embryos from E6.5 to E8.5[36] (Supplementary Fig. 4a, b) we classified the transcriptional
143 identity of the cells (Fig. 4a, b). Except for the least abundant cell types, the distribution of cell
144 types was consistent across two biological replicates (Fig. 4c). Expression of known markers
145 confirmed the classification by mapping to *in vivo* data (Supplementary Fig. 4c, Supplementary
146 Table 1). Most cell types belonged to the E8.0 or E8.5 embryo (Supplementary Fig. 4d), which
147 might indicate that *in vitro* differentiation proceeded roughly with the same speed as *in vivo*
148 development.

149 Neuromesodermal progenitors (NMPs) and spinal cord-like cells were the most
150 abundant in both model systems (Fig. 4c). Gastruloids thus already contain cells of the neural
151 lineage, which, however, seem to lack organization (Fig. 1c, inset). To identify the cells
152 forming epithelial structures in XEGs, we used the neural markers *Sox2*, *Pax6* and *Nkx6.1*[26],
153 which we had detected by immunostaining (Supplementary Fig. 1b). We found these markers
154 to be co-expressed in cells classified as "spinal cord" and "brain" in the scRNA-seq data (Fig.
155 4d, Supplementary Fig. 4e), confirming their neural ectoderm identity. While NMPs also
156 expressed *Sox2* and *Nkx6.1*, neuroepithelial structures where clearly distinguishable by the
157 presence of *Pax6* and the absence of *T*.

158 The scRNA-seq results also supported the existence of anteroposterior, as well as
159 dorsoventral patterning. Several anterior and posterior markers were clearly expressed in
160 separate subpopulations (Fig. 4e). Differential gene expression analysis between "spinal cord"
161 cells and other cells in XEGs identified markers of both the dorsal and ventral neural tube (Fig.

162 4e, Supplementary Fig. 5a, Supplementary Table 2). Two sets of genes that were either co-
163 expressed with *Msx1* or *Nrcam*, respectively, showed strong anticorrelation (Fig. 4f, left),
164 which confirmed our immunostaining results (Fig. 2c). Similarly, the averages of canonical
165 dorsal and ventral markers were anti-correlated (Fig. 4f, right), despite individual markers
166 being lowly expressed. A comparison between XEGs and gastruloids revealed that neural
167 ectoderm-like cells expressed more dorsal markers in XEGs (Supplementary Fig. 5b). This
168 dorsal identity was confirmed by mapping the neural ectoderm-like cells to single-cell
169 expression profiles of *in vivo* neural tube[37] (Supplementary Fig. 5c). The majority of neural
170 ectoderm-like cells from XEGs turned out to be more similar to dorsal progenitors *in vivo*. All
171 in all, the scRNA-seq results support dorsoventral patterning in XEGs, with a bias towards the
172 dorsal identity, compared to gastruloids.

173 Overall, both model systems showed a diverse cell type distribution, comprising a
174 variety of mesodermal as well as anterior cell types. Thus, XEG cells are not globally biased
175 towards the neural fate, as occurring in other protocols for induction of neural epithelia[12,28,38].
176 On the contrary, XEGs even contained a bigger proportion of mesoderm-like cells. While
177 paraxial, intermediate and somitic mesoderm were present in both model systems, only XEGs
178 contained primitive streak, nascent mesoderm, pharyngeal mesoderm and hematoendothelial
179 progenitors (Fig. 4c, Supplementary Fig. 6a). To confirm the presence of mesodermal cell types
180 in XEGs, we focused on two genes, *Tbx6* and *Pax2*, which are markers of nascent and
181 intermediate mesoderm, respectively. Our single-cell RNA-seq data showed expression of both
182 genes in subpopulations of XEG cells (Supplementary Fig. 6b) and immunostaining confirmed
183 their presence (Supplementary Fig. 6c). However, we did not observe any tissue-level
184 organization of those cells in XEGs. Taken together, these results suggest that the XEN-derived
185 cells in XEGs also have an effect on the mesodermal cell population, which, in turn, could
186 potentially pattern the neuroepithelial tissues.

187

188 **Most XEN cells become VE-like in XEGs**

189 Compared to gastruloids, XEGs additionally contained extraembryonic endoderm cell types
190 (Fig. 4c). By using GFP-expressing XEN cells in XEGs (Supplementary Fig 7a), we
191 established that those cell types were exclusively differentiated from XEN cells. By
192 comparison to undifferentiated XEN cells, which were spiked into the scRNA-seq samples, we
193 studied the transcriptional changes in XEN-derived cells. Undifferentiated XEN cells mostly
194 mapped to PE[36] (Fig. 5a, Supplementary Fig. 7b), consistent with a previous study[39,40]. Their
195 derivatives in XEGs mapped to multiple kinds of extraembryonic endoderm: PE, embryonic
196 VE and extraembryonic VE. Interestingly, some also mapped to gut, reminiscent of the
197 contribution of VE to the gut *in vivo*[19,41]. The identification of those cell types was confirmed
198 by mapping our scRNA-seq data to an endoderm-focused scRNA-seq dataset[41]
199 (Supplementary Fig. 7c,d). Quantification revealed that, on average, 8% of the initially PE-like
200 XEN cells acquired a gut-like and 66% a VE-like transcriptomic profile (29% embryonic VE,
201 37% extraembryonic VE) when co-cultured in XEGs. However, 25% retained a PE-like
202 transcriptome (Fig. 5a). Differential gene expression analysis between undifferentiated XEN
203 cells and XEN-derivatives revealed several differences (Supplementary Fig. 7e,
204 Supplementary Table 3). PE markers were less expressed in XEN-derivatives, while VE
205 markers were highly expressed, suggesting that most XEN cells differentiate from at PE to a
206 VE-like state in XEGs. To validate this finding experimentally, we performed single-molecule
207 FISH of the PE marker *Fst*[42], the VE marker *Spink1*[43] and the pan-extraembryonic endoderm
208 marker *Dab2*[44] (Fig. 5b). This measurement showed that XEN-derived cells in XEGs only
209 expressed *Dab2* and *Spink1*, while undifferentiated XEN cells broadly co-expressed all
210 markers. Some XEN cells in XEGs were also highly expressing E-cadherin, known to be
211 expressed in VE[45] (Fig. 5c). However, the more anterior VE marker *Hhex*[46] was not detected

212 by single-molecule FISH (Fig. 5d). Exposing undifferentiated XEN cells to CHIR in the same
213 way as XEGs did not cause differentiation (Fig. 5d), which suggests that the interaction with
214 mESCs plays a role.

215 Taken together, these results suggest that XEGs mimic elements of embryo
216 organization *in vivo*, where the VE is in direct contact with the embryo proper. While
217 undifferentiated XEN cells have both PE and VE characteristics, the majority (66%) of these
218 cells becomes more VE-like, due to the presence of mESCs.

219

220 **XEN cells guide symmetry breaking by local inhibition of WNT signaling**

221 Although XEN-derived cells in XEGs did not express canonical AVE markers (Supplementary
222 Fig. 4c), we were wondering if they might effectively carry out an AVE-like patterning
223 function. XEN cells always formed the outermost layer (Fig. 1b, Supplementary Fig. 1f),
224 resembling *in vivo* organization. Focusing on XEGs partially covered with XEN cells, we
225 observed that epithelial structures were always adjacent to the XEN cells, while the T-positive
226 population was on the opposite side (Supplementary Fig. 1f). Notably, this organization was
227 already established at 72 h, when aggregates are still spherical (Fig. 6a). This observation
228 suggested that XEN cells guide the symmetry breaking by a local effect on the adjacent mESCs.
229 We speculated that this effect might be mediated by a basement membrane produced by the
230 XEN cells. As established above, cells were polarized early during XEG development, prior to
231 forming a columnar epithelium (Supplementary Fig. 1c, d). This epithelium was supported by
232 a basement membrane containing laminin and collagen (Fig. 6b, c) which were mostly
233 produced by the XEN cells (Supplementary Fig. 8a, top-right). It has been demonstrated
234 previously, for small aggregates of mESCs, that the presence of an extracellular matrix can be
235 sufficient for polarization and lumen formation[27,28,38]. Growing gastruloids in Geltrex did

236 induce the formation of inner cavities; however, we did not observe a columnar epithelium
237 (Supplementary Fig. 8b).

238 Since an extracellular matrix was not sufficient to obtain neuroepithelial structures, we
239 were wondering, which other mechanisms might play a role. We observed that gastruloids
240 grown in medium conditioned by XEN cells, did not elongate and had a T-positive cell
241 population that was restricted to the center of the aggregate (Fig. 6d). Thus, we reasoned that
242 diffusible factors produced by the XEN cells might have a role in the formation of the
243 neuroepithelial structures. We hypothesized that the WNT inhibitor DKK1, which is expressed
244 by the XEN cells (Fig. 6e; Supplementary Fig. 8a, bottom-right), might be one of those factors.
245 *In vivo*, DKK1 is expressed by the AVE and limits the growth of the primitive streak[47]. Notably,
246 other factors known to act in this process (CER1, LEFTY1) are not expressed in XEGs (Fig.
247 6e, Supplementary Fig. 4c). Growing gastruloids in the presence of DKK1 resulted in a round
248 morphology, with the T-positive cells confined to the center, as observed for XEN-conditioned
249 medium (Fig. 6f, Supplementary Fig. 8d). Factors limiting the primitive streak expansion *in*
250 *vivo* are also known to preserve the anterior part of the epiblast and are thereby necessary for
251 proper ectoderm domain differentiation[48]. Thus, we wanted to explore, if DKK1 could have a
252 similar role in XEGs and bias differentiation towards the ectodermal lineage. Growing XEGs
253 with the DKK1 inhibitor WAY-262611[49] led to a suppression of epithelial structures (Fig. 6g,
254 Supplementary Fig. 8e). Notably, XEGs treated with the DKK1 inhibitor resembled
255 gastruloids, showing elongated shapes but no epithelial structures. Since growing XEGs
256 without CHIR resulted in similar epithelial structures as in regular XEGs (Supplementary Fig.
257 8c), XEN cells likely suppress pre-existing, low-level endogenous WNT activity[6,50]. Finally,
258 we noticed that XEN-derived cells highly express BMPs (Supplementary Fig. 8a, bottom-right)
259 and that several of the dorsal markers expressed in XEGs, are induced by BMP signaling

260 (Supplementary Table 4). Thus, XEN-derived cells might also contribute to the dorsal
261 patterning of the neural progenitors-like cells in XEGs.
262 All combined, our experiments suggest that XEN cells guide symmetry-breaking by
263 local inhibition of cell differentiation into a T-positive population. Diffusible factors, including
264 DKK1, and the presence of a basement membrane both seem to contribute to the formation of
265 the neuroepithelial structures.
266

267 Discussion

268 In this study we explored how the interaction between embryonic and extraembryonic cells in
269 a multicellular *in vitro* system can lead to the formation of neuroepithelial tissue. The observed
270 dynamics and organization of the neuroepithelia in XEGs is clearly different from the
271 formation of the neural tube *in vivo*, which occurs via two distinct mechanisms[51]. During
272 primary neurulation, the main part of the neural tube is formed by the folding of the neural
273 plate, an epithelial sheet of neural ectoderm cells. Secondary neurulation, which gives rise to
274 the most posterior part of the neural tube, works differently: mesenchymal cells condense to
275 an epithelial rod which cavitates to form a tube[52,53]. The two parts of the tube are then connected
276 during junctional neurulation[54]. While we did not observe cell rearrangements characteristic of
277 primary neurulation, the rosette formation seen in XEGs was reminiscent of secondary
278 neurulation[51], which gives rise to the posterior neural tube. Nevertheless, we were able to
279 differentiate XEGs towards neural tissue that showed layered organization reminiscent of the
280 cortex, which derives from the anterior neural tube. The neuroepithelia in 96 h XEGs are
281 therefore likely still plastic and would need additional time and signaling inputs to become
282 fully specified.

283 The recently reported Trunk-Like Structures (TLS)[55], another gastruloid-derived model
284 system, also produce neural tube-like tissues, together with mesodermal tissue resembling
285 somites. Notably, TLS are formed exclusively from mESCs and are grown in Matrigel with
286 additional exogenous signaling cues (BMP signaling inhibitor LDN193189 and CHIR).
287 Another recent approach uses BMP4-treated ESCs as signaling centers to elicit neural tube-
288 like tissues and other embryonic structures in untreated ESCs[13].

289 The fact that the majority of XEN cells becomes VE-like in XEGs clearly shows that
290 there are reciprocal interactions between the co-differentiating, embryonic and extraembryonic
291 cells. This observation supports the notion that such interactions are necessary for proper
292 development, as previously observed *in vivo*[19,56]. Thus, XEN cells represent a potential way to
293 augment existing developmental *in vitro* systems, by providing a basement membrane and
294 extraembryonic signaling inputs.

295 Finally, with their large diversity of cell types, XEGs could be a starting point for
296 developing more complex models containing all three germ layers as well as extraembryonic
297 cells. Specifically, the CD31 positive endothelial cells observed in the cerebral organoids
298 obtained from XEGs might be able to form a vascular network if additional signaling cues are
299 given[57].

300 In conclusion, in this study we showed how the morphogenic potential of heterotypic
301 cell-cell interactions can be leveraged to enhance the organization of multicellular *in vitro*
302 systems.

303

304 Methods

305 Experimental methods

306 Cell culture

307 All cell lines were routinely cultured in KO DMEM medium (Gibco) supplemented with 10%
308 ES certified FBS (Gibco), 0.1 mM 2-Mercaptoethanol (Sigma-Aldrich), 1 × 100 U/mL
309 penicillin/streptomycin, 1x MEM Non-Essential Amino Acids (Gibco), 2 mM L-glutamine
310 (Gibco), 1000 U/mL mouse LIF (ESGRO). Cells were passaged every other day and replated
311 in tissue-culture treated dishes coated with gelatin. E14 mouse ES cells were provided by
312 Alexander van Oudenaarden. The *Sox1*^{GFPiresPac} mouse ES cell line was created by Mario
313 Stavridis and Meng Li in the group of Austin Smith[58] and provided by Sally Lowell. XEN and
314 XEN-*eGFP* were provided by Christian Schröter[40]. All cell lines were regularly tested for
315 mycoplasma infection. The ES-mCherry-GPI cell line was obtained by introducing a mCherry-
316 GPI transgene in the *Pdgfra*$^{H2B\text{-}GFP}$ cell line, provided by the group of Anna-Katerina
317 Hadjantonakis[59].
318

319 ## Differentiation

320 ### Gastruloids

321 The gastruloid differentiation protocol was adapted from van den Brink et al. [5]. ES cells were
322 collected from tissue-culture treated dishes by trypsinization, gentle trituration with a pipet and
323 centrifugation (1200 r.p.m., 3 min). After collection, cells were resuspended in 2 mL of freshly
324 prepared, prewarmed N2B27 medium: DMEM/F12 (Life technologies) supplemented with 0.5
325 × N2 supplement (Gibco), 0.5 × B27 supplement (Gibco), 0.5 mM L-glutamine (Gibco),
326 1 × 100 U/mL penicillin/streptomycin (Gibco), 0.5 × MEM Non-Essential Amino Acids
327 (Gibco), 0.1 mM 2-Mercaptoethanol (Sigma-Aldrich). Cells were counted to determine the cell
328 concentration. For gastruloids, 200 ES cells were seeded in 40 µL of N2B27 in each well of a
329 round-bottom low-adherence 96-well plate. 48 h after seeding, 150 µL of prewarmed N2B27
330 supplemented with 3 µM of GSK3 inhibitor (CHIR99021, Axon Medchem) was added to each
331 well. 72 h after seeding, 150 µL of medium was removed from each well and replaced by 150

332 μL of preheated N2B27. Gastruloids were collected at 96 h after seeding and fixed with 4%
333 paraformaldehyde (PFA, Alfa Aesar) overnight at 4 ºC.
334 For the experiments with gastruloids grown in Geltrex, cell aggregates were collected at 24 h,
335 48 h and 72 h and embedded into LDEV-Free, hESC-Qualified, reduced growth factor Geltrex
336 (Gibco) in culture dishes for the rest of the procedure. Only the gastruloids transferred at 72 h
337 showed robust growth. At 96 h, culture dishes were covered with ice-cold PBS and placed on
338 a shaker at 4 ºC for 10 min. Gastruloids were gently collected by pipetting and washed three
339 times by centrifugation in ice-cold PBS to remove the gel, then fixed with 4% PFA overnight
340 at 4 ºC.

341 **XEN Enhanced Gastruloids (XEGs)**

342 ES and XEN cells were collected from tissue-culture treated dishes by trypsinization, gentle
343 trituration with a pipet and centrifugation (1200 r.p.m., 3 min). After collection, cells were
344 resuspended in 2 mL of fresh and prewarmed N2B27 medium. Cells were counted to determine
345 cell concentration. For XEGs, several ratios of XEN and ES cells were tested (1:1, 1:2, 1:3,
346 1:4, 1:5) and compared with the regular gastruloid condition (0:1). The total number of cells
347 was fixed at 200. Over two separate experiments, the proportion of organoids showing T
348 staining and epithelial structures was quantified (total number of embryonic organoids
349 1:1=179, 1:2=143, 1:3=143, 1:4=140, 0:1=130) and the optimal ratio was determined to be 1:3
350 (Supplementary Fig. 1e,f). A total of 200 cells (150 ES cells and 50 XEN cells) was seeded in
351 40 μL of N2B27 in each well of a round-bottom low-adherence 96-well plate. 48 h after
352 seeding, 150 μL of prewarmed N2B27 supplemented with 3 μM of GSK3 inhibitor
353 (CHIR99021, Axon Medchem) was added to each well. 72 h after seeding, 150 μL of medium
354 was removed from each well and replaced by 150 μL of prewarmed N2B27. XEGs were
355 collected at 96 h after seeding and fixed with 4% PFA overnight at 4 ºC.

356 For the experiment of XEGs grown without GSK3 inhibitor, cells were seeded as usual. At 48
357 h, 150 µL of preheated N2B27 was added to each well. At 72 h, 150 µL of medium was
358 removed from each well and replaced by 150 µL of prewarmed N2B27. XEGs were collected
359 at 96 h after seeding.
360 For the smFISH control experiments, XEN cells were seeded at low density in N2B27 medium.
361 At 48 h the medium was replaced by prewarmed N2B27 supplemented with 3 µM of GSK3
362 inhibitor. 72 h after seeding, the medium was replaced with prewarmed N2B27. Cells were
363 fixed at 96 h with 4% PFA for 1 h at 4 ºC.
364 **Neural differentiation**
365 For neural differentiation, a protocol for creating cerebral organoids was adapted from
366 Lancaster et al. [35]. Instead of collecting XEGs at 96 h, the medium was replaced by cerebral
367 organoid differentiation medium: DMEM-F12 (Life technologies), Neurobasal (Gibco), 0.5 ×
368 B27 supplement containing vitamin A (Gibco), 0.5 × N2 supplement (Gibco), 2.5 µM/mL
369 Insulin, 2mM L-glutamine (Gibco), 0.5 × MEM-Non-Essential Amino Acids (Gibco), 1 × 100
370 U/mL penicillin-streptomycin and 0.05 mM 2-Mercaptoethanol (Sigma-Aldrich). At 168 h,
371 aggregates were collected and transferred, with fresh medium, into 10 cm dishes on an orbital
372 shaker installed in the incubator (85 r.p.m.). Aggregates were grown until 192 h (8 days) during
373 which medium was refreshed every other day until collection. Collected aggregates were fixed
374 with 4% PFA for 48 h at 4 ºC.
375
376 ## Signaling experiments
377 In the signaling experiments with XEGs, aggregates were treated between 72 h and 96 h with
378 either LDN193189 (BMPi, 100 nM, Reagents Direct), a potent BMP pathway inhibitor,
379 Purmorphamine (1 µM, STEMCELL Technologies), a small molecule agonist of the hedgehog
380 pathway, Retinoic acid (RA, 100 nM, Sigma-Aldrich) or DMSO (0.1% final concentration,

381 Sigma Aldrich) as a vehicle control. For this experiment, the XEGs were allowed to grow for
382 an additional 48 h before fixation (144 h total growth) and preparation for staining (see
383 Immunostaining).
384 DKK1 signaling pathways perturbation was performed in two ways, using DKK1 (Sigma-
385 Aldrich) for activation in gastruloids and Way262611 (Sigma-Aldrich) for inhibition in XEGs.
386 Gastruloids and XEGs were seeded according to the usual protocols. At 24 h, 40 µL of N2B27
387 supplemented with various concentration of DKK1 or Way262611 respectively, were added to
388 each well. Next steps of the protocol were performed using N2B27 supplemented with DKK1
389 or Way262611. Aggregates were fixed at 96 h with 4% PFA overnight at 4 ºC.
390

391 ## Immunostaining

392 **Fixation and blocking**

393 After collection, gastruloids and XEGs were fixed in 4% PFA at 4 °C overnight. Tissue
394 resulting from the cerebral organoid protocol was fixed under the same conditions, but for 48
395 h. After fixation, samples were washed three times in washing solution (PBS, 1% bovine serum
396 albumin (BSA)) and incubated at 4 °C in blocking buffer (PBS, 1% BSA, 0.3% Triton-X-100)
397 for a minimum of 16 h. Samples for smFISH were washed 3 times in PBS after fixation and
398 stored in 70% ethanol at 4 °C. To stain E14 cells for pluripotency markers, cells in suspension
399 were fixed for 30 min in 4% PFA at 4 °C, washed three times in washing solution at RT and
400 incubated in blocking buffer for 1 h at 4 °C.
401

402 **Whole-mount immunolabeling and clearing**

403 Immunolabeling and clearing of gastruloids and XEGs were based on the protocol described
404 by Dekkers et al., [60]. Briefly, after fixation and blocking, samples were incubated with primary
405 antibodies at 4 °C overnight on a rolling mixer (30 r.p.m.) in organoid washing buffer (OWB)

406 (PBS, 2% BSA, 0.1% Triton-X-100) supplemented with 0.02% sodium dodecyl sulfate (SDS),
407 referred to as OWB-SDS. The following primary antibodies were used: rat anti-SOX2 (1:200,
408 14-9811-82, Thermo Fisher Scientific), goat anti-T (1:200, sc-17745, Santa Cruz
409 Biotechnology), goat anti-T (1:100, AF2085, R&D systems), mouse anti-DAB2 (1:100,
410 610464, BD Biosciences). The next day, samples were washed three times for 2 h in OWB-
411 SDS at RT, followed by incubation with secondary antibodies (donkey anti-goat Alexa Fluor
412 488 (1:200, A-11055, Thermo Fisher Scientific), donkey anti-rat Alexa Fluor 488 (1:200, A-
413 21208, Thermo Fisher Scientific), donkey anti-goat Alexa Fluor 555 (1:200, A-21432, Thermo
414 Fisher), donkey anti-mouse Alexa Fluor 555 (1:200, A-31570, Thermo Fisher Scientific),
415 chicken anti-rat Alexa Fluor 647 (1:200, A-21472, Thermo Fisher Scientific)) and 4',6-
416 diamidino-2-phenylindole (DAPI, 1 µg/mL, Merck) in OWB-SDS at 4 °C overnight on a
417 rolling mixer (30 r.p.m.), protected from light. Finally, samples were washed three times for 2
418 h in OWB-SDS at RT. Clearing was performed by incubation in fructose-glycerol clearing
419 solution (60% vol/vol glycerol, 2.5 M fructose) for 20 min at RT. Samples were imaged directly
420 after clearing or stored at 4 °C in the dark.
421
422 **Cryosectioning and immunolabeling of sections**
423 Prior to cryosectioning, fixed and blocked samples were incubated sequentially in sucrose
424 solutions (10, 20 and 30%) for 30 min (gastruloids and XEGs) or 2 h (cerebral organoids) at
425 27 °C, and embedded in optimal cutting temperature (OCT) compound. Samples in OCT were
426 placed on dry ice for rapid freezing, and stored at -80 °C prior to cryosectioning. Samples were
427 cut to cryosections (10 µm thickness) using a cryostat (Thermo Fisher Scientific, USA) and
428 cryosections were placed on poly-L-lysine coated glass slides (Merck). The slides were stored
429 directly at -80 °C. For immunofluorescence staining, slides were thawed and rinsed with PBS
430 for 10 min at RT to dissolve the OCT. Subsequently, slides were incubated overnight at 4 °C

431 with the following primary antibodies diluted in blocking buffer: rat anti-SOX2 (1:200, 14-
432 9811-82, Thermo Fisher Scientific), goat anti-T (1:200, sc-17745, Santa Cruz Biotechnology),
433 mouse anti-N-cadherin (1:200, 33-3900, Thermo Fisher Scientific), rabbit anti-E-cadherin
434 (1:200, 3195, Cell Signaling Technology), rabbit anti-PAX6 (1:100 (cerebral organoids) or
435 1:200 (gastruloids, XEGs), 42-6600, Thermo Fisher Scientific), mouse anti-NKX6.1 (1:200,
436 F55A12, Developmental Studies Hybridoma Bank), rabbit anti-NKX6.1 (1:200, HPA036774,
437 Merck), mouse anti-TUJ1 (1:200, 801202, BioLegend), rabbit anti-CD31 (1:50, ab28364,
438 Abcam), rabbit anti-GATA6 (1:200, PA1-104, Thermo Fisher Scientific), goat anti-GATA6
439 (1:200, AF1700, R&D Systems), rabbit anti-Laminin (1:200, PA1-16730, Thermo Fisher
440 Scientific), mouse anti-OCT4 (1:200, MA1-104, Thermo Fisher Scientific). The next day, the
441 slides were washed twice for 10 min in PBS at RT. Subsequently, the slides were incubated
442 with secondary antibodies (donkey anti-goat Alexa Fluor 488 (1:200, A-11055, Thermo Fisher
443 Scientific), donkey anti-rat Alexa Fluor 488 (1:200, A-21208, Thermo Fisher Scientific),
444 donkey anti-goat Alexa Fluor 555 (1:200, A-21432, Thermo Fisher), donkey anti-mouse Alexa
445 Fluor 555 (1:200, A-31570, Thermo Fisher Scientific), chicken anti-rat Alexa Fluor 647 (1:200,
446 A-21472, Thermo Fisher Scientific), donkey anti-rabbit Alexa Fluor 647 (1:200, A-31573,
447 Thermo Fisher Scientific)) and DAPI (1 µg/mL, Merck) in blocking buffer for 4 h at 4 °C, and
448 washed three times for 10 min at RT. Slides were mounted in ProLong™ Gold Antifade
449 Mountant (Thermo Fisher Scientific) and imaged after 24-48 h.

450 **Immunolabeling of E14 cells**

451 After fixation and blocking, E14 cells were incubated with the following primary antibodies in
452 blocking buffer overnight at 4 °C: rat anti-SOX2 (1:200, 14-9811-82, Thermo Fisher
453 Scientific) and mouse anti-OCT4 (1:200, MA1-104, Thermo Fisher Scientific). The next day,
454 cells were washed three times in washing solution for 5 min at RT and incubated with
455 secondary antibodies (donkey anti-rat Alexa Fluor 488 (1:200, A-21208, Thermo Fisher

456 Scientific) and donkey anti-mouse Alexa Fluor 555 (1:200, A-31570, Thermo Fisher
457 Scientific)) and DAPI (1 µg/mL, Merck) in blocking buffer for 3 h at 4 °C. Finally, the cells
458 were washed three times in washing solution for 5 min at RT and imaged directly.
459

460 **Single-molecule fluorescence in-situ hybridization (smFISH)**

461 smFISH was performed as described previously[61]. Briefly, samples were fixed with PFA and
462 stored in 70% ethanol, as described above. Custom designed smFISH probes for *Dab2*, *Fst*,
463 *Hhex* and *Spink1* (BioCat, Supplementary Table 5), labeled with Quasar 570, CAL Fluor Red
464 610, or Quasar 670, were incubated with the samples overnight at 30 °C in hybridization buffer
465 (100 mg/mL dextran sulfate, 25% formamide, 2X SSC, 1 mg/mL E.coli tRNA, 1 mM vanadyl
466 ribonucleoside complex, 0.25 mg/mL BSA; Thermo Fisher Scientific). Samples were washed
467 twice for 30 min at 30 °C with wash buffer (25% formamide, 2X SSC). The wash buffer was
468 supplemented with DAPI (1 µg/mL) in the second wash step. All solutions were prepared with
469 RNAse-free water. Finally, the samples were mounted in ProlongGold (Life Technologies) and
470 imaged when hardened (sections) or immediately (ibidi dishes). All components are from
471 Sigma-Aldrich unless indicated.
472

473 **Imaging**

474 Fixed and stained samples were imaged on a Nikon Ti-Eclipse epifluorescence microscope
475 equipped with an Andor iXON Ultra 888 EMCCD camera and dedicated, custom-made
476 fluorescence filter sets (Nikon). Primarily, a 10× / 0.3 Plan Fluor DLL objective, a 20× / 0.5
477 Plan Fluor DLL objective, or a 40× / 1.3 Super Fluor oil-immersion objective (Nikon) were
478 used. To image complete sections of cerebral organoids, multiple adjacent fields of view were
479 acquired and combined using the tiling feature of the NIS Elements software (Nikon). Z-stacks
480 were collected of whole-mount gastruloids and XEGs with distances of 10 µm between planes.

481 For smFISH measurements, z-stacks were collected with a distance of 0.2 μm between planes
482 in four fluorescence channels (DAPI, Quasar 570, CAL Fluor Red 610, Quasar 670) using a
483 100× /1.45 Plan Apo Lambda oil (Nikon) objective. Time lapses to observe the formation of
484 epithelial structures were performed 24 h and 48 h after cell seeding, on XEGs grown from the
485 mCherry-GPI ES cell line. XEGs were transferred to a glass-bottom μ-Slide imaging chamber
486 (ibidi) and imaged every 30 min for 24 h with a Nikon Eclipse Ti C2+ confocal laser
487 microscope (Nikon, Amsterdam, The Netherlands), equipped with lasers at wavelengths 408,
488 488 and 561, an automated stage and perfect focus system at 37°C and 5% CO_2. Images were
489 acquired with a Nikon 20x Dry Plan Apo VC NA 0.75 objective. To track SOX1 expression in
490 gastruloids and XEGs during the 24 h growth after the GSK3 inhibitor pulse, 72 h gastruloids
491 and XEGs grown from the *Sox1*^{GFPiresPac} ES cell line were transferred to a glass-bottom μ-Slide
492 imaging chamber (ibidi) and imaged every 40 min for 24 h, while temperature and CO_2 levels
493 were maintained at 37 °C and 5%, respectively, by a stage top incubator (INUG2-TIZW-SET,
494 Tokai Hit) mounted on the Nikon Ti-Eclipse epifluorescence microscope.
495

496 **Single-cell RNA-seq library preparation and sequencing**

497 For each replicate, 96 pooled gastruloids and 96 pooled XEGs were collected from a round-
498 bottomed low-adherence 96-well plate in 15 mL Falcon tubes and pelleted by gentle
499 centrifugation (500 r.p.m. for 2 min). No final aggregate was excluded from the collection.
500 After washing with cold PBS, samples were resuspended in N2B27. Cells were then
501 dissociated by 5 min incubation in TrypLE (Gibco) and gentle trituration with a pipet,
502 centrifuged and resuspended in 1 mL of cold N2B27. Cells were counted to determine cell
503 number and viability. For the first replicate, ES-mCherry-GPI were spiked in at a frequency of
504 5%. For the second replicate, E14 cells were collected from culture dishes and incubated for
505 30 min at 4 ºC with CITE-seq cell hashing[62] antibody Ab_CD15 (1:200) (Biolegend). XEN-

506 *eGFP* were collected from culture plates and incubated for 30 min at 4 ºC with CITE-seq cell
507 hashing antibody Ab_CD140 (1:200) (Biolegend). In the gastruloid sample, labeled E14 cells
508 were spiked in at a frequency of 5%, whereas in the XEG sample labeled E14 and XEN-*eGFP*
509 were spiked in, both at a frequency of 5%. High viability of the cells in all samples was
510 confirmed before 10X library preparation. Single-cell RNA-seq libraries were prepared using
511 the Chromium Single Cell 3' Reagent Kit, Version 3 Chemistry (10x Genomics) according to
512 the manufacturer's protocol. CITE-seq libraries were prepared according to the CITE-seq
513 protocol from New York Genome Center version 2019-02-13. Libraries were sequenced paired
514 end on an Illumina Novaseq6000 at 150 base pairs.
515

516 # Computational methods

517 ## Analysis of single-cell RNA-sequencing data

518 **Single-cell RNA-seq data pruning and normalization**

519 Cells with a low number of transcripts were excluded from further analysis based on the
520 histograms in Supplementary Fig. 3a (count < 1300 for replicate 1 of the XEG experiment and
521 count < 2300 for the other datasets). Genes expressed in less than 2 cells (across merged
522 replicates) were excluded from further analysis. The final XEG dataset contains 14286 genes
523 and 4591 or 6857 cells for replicate 1 or 2, respectively. The gastruloid dataset contains 14384
524 genes and 4233 or 8363 cells per replicate. The two datasets were normalized using the scran
525 R-package (V 1.10.2[63]). Gene variabilities were calculated (improvedCV2, scran) for each
526 replicate separately, after excluding ribosomal genes [Ribosomal Protein Gene Database,
527 http://ribosome.med.miyazaki-u.ac.jp/], exogenously expressed genes and genes expressing
528 the antibodies used for CITE-seq. The 10% most highly variable genes (HVG) were selected
529 based on variability p-values.

530 **Dimensionality reduction**

531 For each of the two datasets, the two replicates were batch corrected with the fast mutual
532 nearest neighbors (MNN) method implemented in the scran R-package[64], using the union of
533 the 10% HVG of the two replicates and log-transformed normalized counts with d = 120
534 (number of principal components) and k = 50 (number of nearest neighbours). For
535 dimensionality reduction, a uniform manifold approximation and projection (UMAP) was
536 calculated on the batch corrected data using the R-package UMAP (V 0.2.3.1) with n = 50,
537 min_dist = 0.7 and using the cosine distance measure.

538 **Identification of spike-in cells**

539 Cells with any expression of mCherry were annotated as ES (mCherry+). The remaining spike-
540 in cells, E14 (CD15+) and XEN spike-in (CD140+) (see Single-cell RNA-seq library
541 preparation and sequencing), could not be determined by the expression level of the antibody
542 alone. We therefore chose to assign spike-ins based on clusters. For each of the two datasets, a
543 shared nearest neighbor graph was constructed from the batch corrected data (see
544 Dimensionality reduction) with scran using k = 20 and d = 30. Louvain clustering was
545 performed on the constructed graphs with the R-package igraph (V1.2.4.1), which resulted in
546 8 clusters for XEGs and 7 clusters for gastruloids (see Supplementary Fig. 3c). We identified
547 3 out of the 8 clusters in XEGs based on literature markers and spike-in gene expression. One
548 cluster out of these three was mainly comprised of mESCs, due to high Ab_CD15 expression
549 and mCherry positive cells. Cells that had an expression of Ab_CD15 > 50 and were part of
550 this cluster were considered spiked-in E14 and annotated as E14 (CD15+). The other two
551 clusters were both eGFP positive, where one of them had a higher Ab_CD140 expression and
552 was thus annotated as XEN spike-in (Ab_CD140+). The second cluster was annotated as XEN
553 derived (Ab_CD140-). Similarly, for gastruloids, one of the 7 clusters was comprised of mainly
554 mESCs based on literature markers and spike-in gene expression. Cells that had an expression

555 of Ab_CD15 > 100 and were part of this cluster were considered spiked-in E14 and annotated
556 as E14 (CD15+).

557 **Analysis of cell cycle and stress-related genes**

558 For each of the two datasets, cell cycle analysis was performed with the scran package using
559 the cyclone function[65] on the normalized counts. Cells in G2M phase were distributed evenly
560 across all clusters and thus the clustering was not biased by cell cycle. No other separate cluster
561 that consisted entirely of cell cycle related cells appeared.

562 For the analysis of stress-related genes, a list of known stress genes[66] was used to calculate the
563 average standardized expression per cell based on normalized counts. Stress-related genes were
564 mainly found within the spike-in cells and there was no other separate cluster that consisted
565 entirely of highly stressed cells.

566 **Mapping to *in vivo* datasets**

567 Our datasets were mapped to three different *in vivo* datasets.

568 *Pijuan-Sala et al. dataset*

569 The Pijuan-Sala et al. dataset[36], which was downloaded from
570 https://content.cruk.cam.ac.uk/jmlab/atlas_data.tar.gz, consists of 9 timepoints from E6.5 to
571 E8.5. The data was normalized by size factors provided by the authors. Cells with no cell type
572 assignment were excluded from further analysis. The 10% HVG were calculated
573 (improvedCV2, scran package) on the remaining cells excluding sex genes, similar to Pijuan-
574 Sala et al.'s method. Cells in the "mixed_gastrulation" cluster were also excluded. MNN
575 mapping was applied to log-transformed normalized counts of the 10% HVG. First, *in vivo*
576 timepoints were mapped to each other in decreasing order. Then, each of our four datasets was
577 mapped separately to the combined Pijuan-Sala et al. dataset (MNN method with d = 120, k =
578 50). K-nearest-neighbor (knn) assignment was performed in the batch corrected principal
579 component space. For each cell in our datasets, the 50 nearest neighbors in the *in vivo* dataset,

580 based on Euclidean distances, were calculated. Each cell was assigned the most abundant cell
581 type within the knn, if certain distance and confidence score conditions were met. This
582 confidence score was calculated for each cell as the number of the most abundant cell type
583 divided by the total number of neighbors (k=50). A cell was annotated as "Not assigned" if
584 either, the average distance to its nearest neighbor exceeded a certain threshold (determined by
585 the long tail of the histogram of average distances for each of our datasets separately) or the
586 assignment had a confidence score less than 0.5. Additionally, we placed cells in "Not
587 assigned" if they were assigned to clusters with less than 10 cells, or to the cluster "Blood
588 progenitors 2" (because this cluster did not show distinct expression of known literature
589 markers). This resulted in 22 assigned clusters for XEGs and 15 assigned clusters for
590 gastruloids. For each cell in our dataset we calculated the average and the standard deviation
591 of the developmental age of the knn.

592 *Nowotschin et al. dataset*

593 The Nowotschin et al. dataset[41], which was downloaded from https://endoderm-explorer.com/,
594 consists of 6 timepoints from E3.5 to E8.75. The data was normalized (scran) and the 10%
595 HVG were calculated (improvedCV2, scran package). First, MNN was applied to the
596 Nowotschin et al. dataset in increasing order of the timepoints (using log-transformed
597 normalized counts of the 10% HVG, d = 150, k =50). Then, XEN cells from our XEG dataset
598 (XEN spike-ins (CD140+) and XEN derived (CD140-)) were mapped to the MNN-corrected
599 Nowotschin et al. dataset. Knn assignment was performed as described above and resulted in
600 7 assigned clusters.

601 *Delile et al. dataset*

602 The Delile et al. dataset[37], which was downloaded from
603 https://github.com/juliendelile/MouseSpinalCordAtlas, consists of 5 timepoints from E9.5 to
604 E13.5. Cells that had a cell type assignment of "Null" or "Outlier" were excluded from further

605 analysis. The data was normalized (scran) and the 10% HVG were calculated. First, MNN was
606 applied to the Delile et al. dataset in order of increasing timepoints (log-transformed
607 normalized counts of the 10% HVG, d = 120, k =50). Then, we mapped "Spinal cord" cells to
608 the MNN corrected Delile et al. dataset separately for each of our replicates. Knn assignment
609 was performed as described above and resulted in 3 clusters for XEGs and 3 clusters for
610 gastruloids.

611 **Differential expression analysis**

612 For the differential expression test between "spike-in XENs" and "XENs in XEGs" a Welch t-
613 test (implemented in findMarkers, scran R package) was conducted on the normalized log-
614 transformed counts. The test was performed on XEGs from replicate 2. "spike-in XENs" were
615 chosen as the 100 cells with highest Ab_CD140 expression and "XENs in XEGs" were the 100
616 cells with lowest Ab_CD140 expression within the XEN identified cells.

617 For the differential expression test between XEGs and gastruloids, a negative binomial
618 regression was performed (R package edgeR V 3.24.3[67]). Based on the knn assignment to the
619 Pijuan-Sala et al. dataset, all cells annotated as "Spinal cord" were extracted from our four
620 datasets (in XEGs 859 cells in replicate 1 and 166 cells in replicate 2, in gastruloids 2071 cells
621 in replicate 1 and 1882 cells in replicate 2). Raw counts were used for the regression with these
622 four subsets as dummy variables and a variable corresponding to the total number of counts
623 per cell. P-values were obtained for the contrast between XEGs and gastruloids using the
624 average regression coefficients among variables of both replicates.

625 Similarly, for the differential expression test of the "Spinal cord" in XEGs, a negative binomial
626 regression was used. Cells were excluded from the test if either their cell type occurred in less
627 than 10 cells per replicate, or if the cells were annotated as "Not assigned", leaving a total of
628 13 cell types (7742 cells) to be considered. For each cell type and each replicate a dummy
629 variable was created and a variable corresponding to the total number of counts per cell. Then,

630 p-values were obtained for the contrast between the average regression coefficients of the two
631 replicates of the "Spinal cord" cluster and the average regression coefficients of all other
632 variables considered in the test.
633 For all differential expression tests p-values were adjusted for multiple hypothesis testing with
634 the Benjamini-Hochberg method.
635 **Scatter plot of dorsoventral markers**
636 For the scatter plot of canonical markers, we used the average log-transformed normalized
637 expression of 10 canonical dorsal markers (*Pax7, Msx3, Pax3, Gsh2, Msx2, Olig3, Math1,*
638 *Zic1, Msx1, Zic2*) and the average log-transformed normalized expression of 10 canonical
639 ventral markers (*Olig2, Nkx6.1, Nkx2.2, Foxa2, Ncam1, Nrcam, Nkx6.2, Isl1, Fabp7, Hb9*).
640 The solid line is a running average, calculated by sorting the data on ventral marker expression
641 and averaging dorsal marker expression in sliding bins of 50 data points. The scatterplot of
642 Msx1 and Nrcam module expression was calculated similarly, using 10 genes with the highest
643 Spearman correlation with Msx1 or Nrcam, respectively.
644

645 ## Image analysis

646 Image stacks of whole-mount immunostained gastruloids and XEGs, and images of
647 immunostained sections were pre-processed by background subtraction (rolling ball, radius: 50
648 pixels = 65 μm (10× objective), 32 μm (20× objective) or 16 μm (40× objective)) in the
649 channels that showed autofluorescent background using ImageJ[68]. When background
650 subtraction in images of sections did not result in proper removal of autofluorescent
651 background signal, the Enhance Local Contrast (CLAHE) tool was used in ImageJ[68]. smFISH
652 image stacks were pre-processed by applying a Laplacian of a Gaussian filter ($\sigma = 1$) over the
653 smFISH channels using scikit-image (v0.16.1) [69]. For all image stacks, a maximum projection

654 was used to obtain a 2D representation. To show a single object per image, images were
655 cropped around the object of interest.

References

1. Simunovic, M. & Brivanlou, A. H. Embryoids, organoids and gastruloids: new approaches to understanding embryogenesis. *Development* **144,** 976–985 (2017).
2. Vianello, S. & Lutolf, M. P. Understanding the Mechanobiology of Early Mammalian Development through Bioengineered Models. *Developmental Cell* **48,** 751–763 (2019).
3. Shahbazi, M. N., Siggia, E. D. & Zernicka-Goetz, M. Self-organization of stem cells into embryos: A window on early mammalian development. *Science* **364,** 948–951 (2019).
4. Kamm, R. D. *et al.* Perspective: The promise of multi-cellular engineered living systems. *APL Bioengineering* **2,** (2018).
5. van den Brink, S. C. *et al.* Symmetry breaking, germ layer specification and axial organisation in aggregates of mouse embryonic stem cells. *Development* **141,** 4231–4242 (2014).
6. Turner, D. A. *et al.* Anteroposterior polarity and elongation in the absence of extra-embryonic tissues and of spatially localised signalling in gastruloids: mammalian embryonic organoids. *Development* **144,** 3894–3906 (2017).
7. Beccari, L. *et al.* Multi-axial self-organization properties of mouse embryonic stem cells into gastruloids. *Nature* 1 (2018). doi:10.1038/s41586-018-0578-0
8. van den Brink, S. C. *et al.* Single-cell and spatial transcriptomics reveal somitogenesis in gastruloids. *Nature* **141,** 4231–5 (2020).

9. Warmflash, A., Sorre, B., Etoc, F., Siggia, E. D. & Brivanlou, A. H. A method to recapitulate early embryonic spatial patterning in human embryonic stem cells. *Nature Methods* **11,** 847–854 (2014).

10. Moris, N. *et al.* An in vitro model of early anteroposterior organization during human development. *Nature* **582,** 410–415 (2020).

11. Sozen, B. *et al.* Self-assembly of embryonic and two extra-embryonic stem cell types into gastrulating embryo-like structures. *Nature Cell Biology* **20,** 979–989 (2018).

12. Haremaki, T. *et al.* Self-organizing neuruloids model developmental aspects of Huntington's disease in the ectodermal compartment. *Nature Biotechnology* **37,** 1198–1208 (2019).

13. Xu, P.-F. *et al.* Construction of a mammalian embryo model from stem cells organized by a morphogen signalling centre. *Nature Communications* **12,** 3277–22 (2021).

14. Pfister, S., Steiner, K. A. & Tam, P. P. L. Gene expression pattern and progression of embryogenesis in the immediate post-implantation period of mouse development. *Gene Expression Patterns* **7,** 558–573 (2007).

15. Harrison, S. E., Sozen, B., Christodoulou, N., Kyprianou, C. & Zernicka-Goetz, M. Assembly of embryonic and extra-embryonic stem cells to mimic embryogenesis in vitro. *Science* eaal1810 (2017). doi:10.1126/science.aal1810

16. Rivron, N. C. *et al.* Blastocyst-like structures generated solely from stem cells. *Nature* **557,** 106–111 (2018).

17. Mathew, B. *et al.* Mouse ICM Organoids Reveal Three-Dimensional Cell Fate Clustering. *Biophys. J.* **116,** 127–141 (2019).

18. Hogan, B. L., Cooper, A. R. & Kurkinen, M. Incorporation into Reichert's membrane of laminin-like extracellular proteins synthesized by parietal endoderm cells of the mouse embryo. *Developmental biology* **80,** 289–300 (1980).

19. Kwon, G. S., Viotti, M. & Hadjantonakis, A.-K. The endoderm of the mouse embryo arises by dynamic widespread intercalation of embryonic and extraembryonic lineages. *Developmental Cell* **15,** 509–520 (2008).

20. Nowotschin, S., Hadjantonakis, A.-K. & Campbell, K. The endoderm: a divergent cell lineage with many commonalities. *Development* **146,** dev150920 (2019).

21. Madabhushi, M. & Lacy, E. Anterior visceral endoderm directs ventral morphogenesis and placement of head and heart via BMP2 expression. *Developmental Cell* **21,** 907–919 (2011).

22. Bedzhov, I. *et al.* Development of the anterior-posterior axis is a self-organizing process in the absence of maternal cues in the mouse embryo. *Cell Research* **25,** 1368–1371 (2015).

23. Hatta, K. & Takeichi, M. Expression of N-cadherin adhesion molecules associated with early morphogenetic events in chick development. *Nature* **320,** 447–449 (1986).

24. Punovuori, K. *et al.* N-cadherin stabilises neural identity by dampening anti-neural signals. *Development* **146,** dev183269 (2019).

25. Tsuda, S. *et al.* FAK-mediated extracellular signals are essential for interkinetic nuclear migration and planar divisions in the neuroepithelium. *Journal of Cell Science* **123,** 484–496 (2010).

26. Jessell, T. M. Neuronal specification in the spinal cord: inductive signals and transcriptional codes. *Nature Reviews Genetics* **1,** 20–29 (2000).

27. Bedzhov, I. & Zernicka-Goetz, M. Self-Organizing Properties of Mouse Pluripotent Cells Initiate Morphogenesis upon Implantation. *Cell* **156,** 1032–1044 (2014).

28. Meinhardt, A. *et al.* 3D Reconstitution of the Patterned Neural Tube from Embryonic Stem Cells. *Stem Cell Reports* **3,** 987–999 (2014).

29. Pevny, L. H., Sockanathan, S., Placzek, M. & Lovell-Badge, R. A role for SOX1 in neural determination. *Development* **125,** 1967–1978 (1998).

30. Olivera-Martinez, I. *et al.* Major transcriptome re-organisation and abrupt changes in signalling, cell cycle and chromatin regulation at neural differentiation in vivo. *Development* **141,** 3266–3276 (2014).

31. Di-Gregorio, A. *et al.* BMP signalling inhibits premature neural differentiation in the mouse embryo. *Development* **134,** 3359–3369 (2007).

32. Dessaud, E., McMahon, A. P. & Briscoe, J. Pattern formation in the vertebrate neural tube: a sonic hedgehog morphogen-regulated transcriptional network. *Development* **135,** 2489–2503 (2008).

33. Maden, M. Retinoid signalling in the development of the central nervous system. *Nat. Rev. Neurosci.* **3,** 843–853 (2002).

34. Ericson, J. *et al.* Pax6 controls progenitor cell identity and neuronal fate in response to graded Shh signaling. *Cell* **90,** 169–180 (1997).

35. Lancaster, M. A. *et al.* Cerebral organoids model human brain development and microcephaly. *Nature* **501,** 373–379 (2013).

36. Pijuan-Sala, B. *et al.* A single-cell molecular map of mouse gastrulation and early organogenesis. *Nature* **566,** 490–495 (2019).

37. Delile, J. *et al.* Single cell transcriptomics reveals spatial and temporal dynamics of gene expression in the developing mouse spinal cord. *Development* **146,** dev.173807 (2019).

38. Ranga, A. *et al.* Neural tube morphogenesis in synthetic 3D microenvironments. *Proc. Natl. Acad. Sci. U.S.A.* **113,** E6831–E6839 (2016).

39. Brown, K. *et al.* A comparative analysis of extra-embryonic endoderm cell lines. *PLoS ONE* **5,** e12016 (2010).

40. Kunath, T. *et al.* Imprinted X-inactivation in extra-embryonic endoderm cell lines from mouse blastocysts. *Development* **132,** 1649–1661 (2005).

41. Nowotschin, S. *et al.* The emergent landscape of the mouse gut endoderm at single-cell resolution. *Nature* **569,** 361–367 (2019).

42. Feijen, A., Goumans, M. J. & van den Eijnden-van Raaij, A. J. Expression of activin subunits, activin receptors and follistatin in postimplantation mouse embryos suggests specific developmental functions for different activins. *Development* **120,** 3621–3637 (1994).

43. Hou, J. *et al.* A systematic screen for genes expressed in definitive endoderm by Serial Analysis of Gene Expression (SAGE). *BMC Developmental Biology* **7,** 92–13 (2007).

44. Yang, D.-H. *et al.* Disabled-2 Is Essential for Endodermal Cell Positioning and Structure Formation during Mouse Embryogenesis. *Developmental biology* **251,** 27–44 (2002).

45. Wang, A. *et al.* Nonmuscle myosin II isoform and domain specificity during early mouse development. *Proc. Natl. Acad. Sci. U.S.A.* **107,** 14645–14650 (2010).

46. Thomas, P. Q., Brown, A. & Beddington, R. S. Hex: a homeobox gene revealing peri-implantation asymmetry in the mouse embryo and an early transient marker of endothelial cell precursors. *Development* **125,** 85–94 (1998).

47. Kimura-Yoshida, C. *et al.* Canonical Wnt signaling and its antagonist regulate anterior-posterior axis polarization by guiding cell migration in mouse visceral endoderm. *Developmental Cell* **9,** 639–650 (2005).

48. Arkell, R. M. & Tam, P. P. L. Initiating head development in mouse embryos: integrating signalling and transcriptional activity. *Open Biology* **2,** 120030–120030 (2012).

49. Pelletier, J. C. *et al.* (1-(4-(Naphthalen-2-yl)pyrimidin-2-yl)piperidin-4-yl)methanamine: a wingless beta-catenin agonist that increases bone formation rate. *J Med Chem* **52,** 6962–6965 (2009).

50. Berge, ten, D. *et al.* Wnt Signaling Mediates Self-Organization and Axis Formation in Embryoid Bodies. *Cell Stem Cell* **3,** 508–518 (2008).

51. Lowery, L. A. & Sive, H. Strategies of vertebrate neurulation and a re-evaluation of teleost neural tube formation. *Mechanisms of Development* **121,** 1189–1197 (2004).

52. Schoenwolf, G. C. Histological and ultrastructural studies of secondary neurulation in mouse embryos. *Am. J. Anat.* **169,** 361–376 (1984).

53. Colas, J. F. & Schoenwolf, G. C. Towards a cellular and molecular understanding of neurulation. *Dev. Dyn.* **221,** 117–145 (2001).

54. Dady, A., Havis, E., Escriou, V., Catala, M. & Duband, J.-L. Junctional neurulation: a unique developmental program shaping a discrete region of the spinal cord highly susceptible to neural tube defects. *J. Neurosci.* **34,** 13208–13221 (2014).

55. Veenvliet, J. V. *et al.* Mouse embryonic stem cells self-organize into trunk-like structures with neural tube and somites. *Science* **370,** (2020).

56. Thomas, P. & Beddington, R. Anterior primitive endoderm may be responsible for patterning the anterior neural plate in the mouse embryo. *Curr. Biol.* **6,** 1487–1496 (1996).

57. Rossi, G. *et al.* Capturing Cardiogenesis in Gastruloids. *Cell Stem Cell* (2020).

58. Ying, Q.-L., Stavridis, M., Griffiths, D., Li, M. & Smith, A. *Conversion of embryonic stem cells into neuroectodermal precursors in adherent monoculture. Nature Biotechnology* **21,** 183–186 (Nature Publishing Group, 2003).

59. Artus, J., Panthier, J.-J. & Hadjantonakis, A.-K. A role for PDGF signaling in expansion of the extra-embryonic endoderm lineage of the mouse blastocyst. *Development* **137,** 3361–3372 (2010).

60. Dekkers, J. F. *et al.* High-resolution 3D imaging of fixed and cleared organoids. *Nat Protoc* **14,** 1756–1771 (2019).

61. Semrau, S. *et al.* FuseFISH: robust detection of transcribed gene fusions in single cells. *Cell Reports* **6,** 18–23 (2014).

62. Stoeckius, M. *et al.* Simultaneous epitope and transcriptome measurement in single cells. *Nature Methods* **14,** 865–868 (2017).

63. Lun, A. T. L., Bach, K. & Marioni, J. C. Pooling across cells to normalize single-cell RNA sequencing data with many zero counts. *Genome Biol.* **17,** 75–14 (2016).

64. Haghverdi, L., Lun, A. T. L., Morgan, M. D. & Marioni, J. C. Batch effects in single-cell RNA-sequencing data are corrected by matching mutual nearest neighbors. *Nature Biotechnology* **36,** 421–427 (2018).

65. Scialdone, A. *et al.* Computational assignment of cell-cycle stage from single-cell transcriptome data. *Methods* **85,** 54–61 (2015).

66. van den Brink, S. C. *et al.* Single-cell sequencing reveals dissociation-induced gene expression in tissue subpopulations. *Nature Methods* **14,** 935–936 (2017).

67. Robinson, M. D., McCarthy, D. J. & Smyth, G. K. edgeR: a Bioconductor package for differential expression analysis of digital gene expression data. *Bioinformatics* **26,** 139–140 (2010).

68. Schneider, C. A., Rasband, W. S. & Eliceiri, K. W. NIH Image to ImageJ: 25 years of image analysis. *Nature Methods* **9,** 671–675 (2012).

69. van der Walt, S. *et al.* scikit-image: image processing in Python. *PeerJ* **2,** e453 (2014).

Acknowledgements

We are thankful to Alfonso Martinez Arias for insightful discussions and feedback on the manuscript. We acknowledge Anna-Katerina Hadjantonakis for helpful input at various stages of the project. We also thank Dr. Sylvia Le Dévédec and Hans de Bont of the Leiden University Cell Observatory for their support in this work. N. B.-C., M. M., P. v.d. B., M. F. and S.S. were supported by the Netherlands Organisation for Scientific Research (NWO/OCW, www.nwo.nl), as part of the Frontiers of Nanoscience (NanoFront) program. E.A. acknowledges support by a Stichting voor Fundamenteel Onderzoek der Materie (FOM, www.nwo.nl) projectruimte grant (16PR1040). M.H. acknowledges support by a Netherlands Organisation for Scientific Research (NWO/OCW, www.nwo.nl) VIDI grant (016.Vidi.189.007). This work was carried out on the Dutch national e-infrastructure with the support of SURF Cooperative. The funders had no role in study design, data collection and analysis, decision to publish, or preparation of the manuscript.

Author contributions

N.B.-C., E.A. and M.H. cultured gastruloids and XEGs. N.B-C., E.A. and M.H. performed signaling experiments and immunostaining and analyzed the resulting images, N.B-C. prepared samples for single-cell RNA sequencing and interpreted the sequencing data, M.M. performed the computational analysis of the single-cell RNA sequencing data, P.v.d.B. contributed to the computational analysis of single-cell RNA sequencing data and carried out the smFISH measurements, M.F. supported all experiments and performed all cryosectioning, N.B.-C., M. M., E.A., P.v.d.B. and M.H. produced figures, N.B.-C., M. M., E.A., P.v.d.B., M.H. and M.F. contributed to the manuscript, T.I., S.T. and S.S. conceived the study and acquired funding. S.S. interpreted the data and wrote the manuscript. All authors discussed the results and commented on the manuscript at all stages.

Competing interest

The authors declare no competing interests.

Data availability

The single-cell RNA sequencing datasets generated in this study are available in the Gene Expression Omnibus repository, GSE141530.

Code availability

Custom R and python code used to analyze the data is available from the authors upon request.

Correspondence and requests for materials

Should be addressed to S.S., S.T., T.I., or M.H.

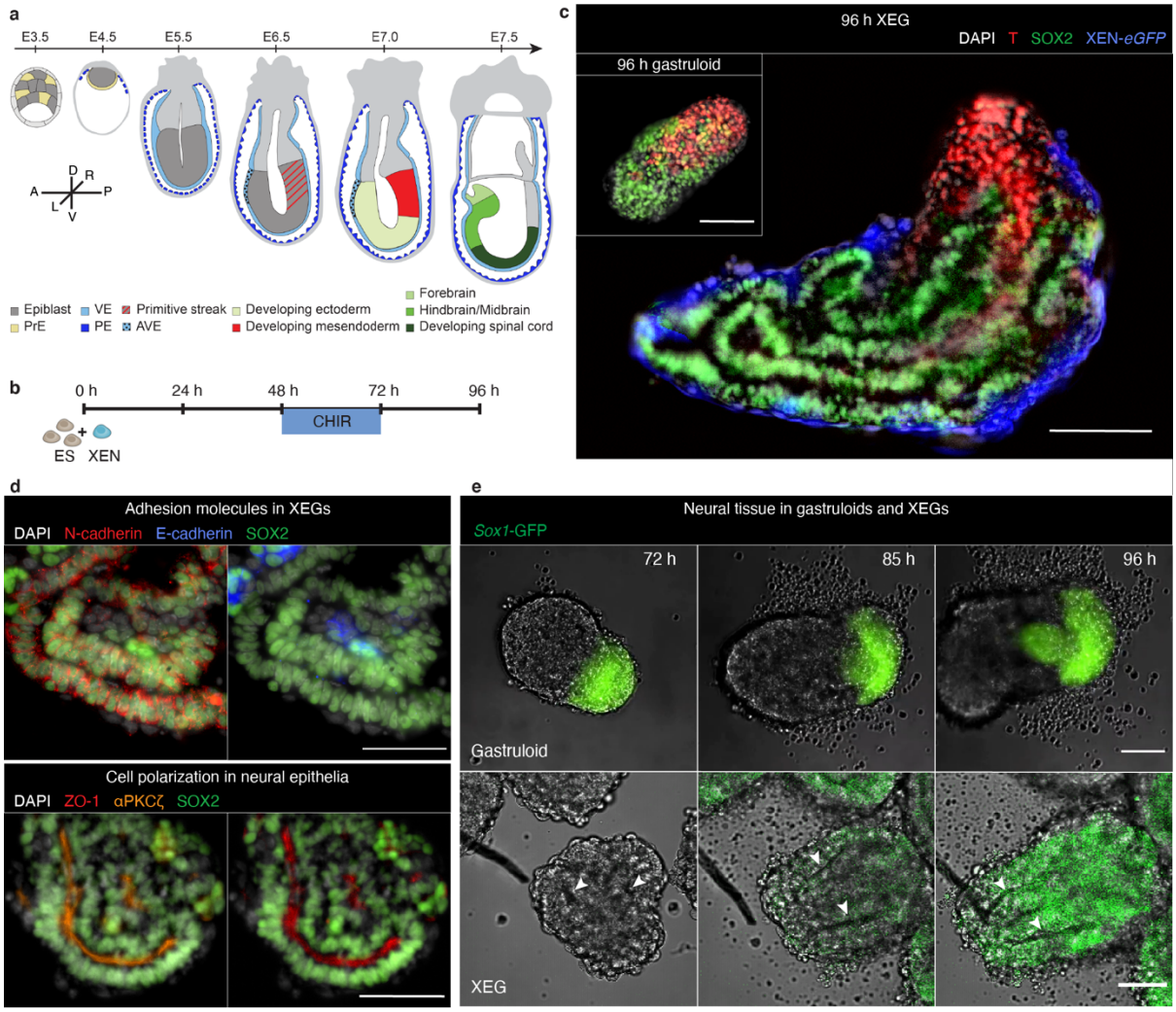

Fig. 1 | XEN cells induce neuroepithelial structures in XEN enhanced gastruloids (XEGs). **a**, Schematic of early mouse embryonic development. Tissues discussed in this manuscript are indicated with color. A: anterior, P: posterior, D: dorsal, V: ventral, L: left, R: right. **b**, Schematic of the culture protocol: at 0 h, 200 cells (150 ESCs and 50 XEN cells) were aggregated; CHIR was added between 48 h and 72 h after cell seeding; cell aggregates were cultured until 96 h. **c**, T and SOX2 expression in XEGs at 96 h (z-projection of whole mount immunostaining). Inset: expression in an aggregate resulting from the standard gastruloid protocol (without XEN cells) at 96 h. Scale bars: 100 µm. **d**, Expression of SOX2, E-cadherin, N-cadherin, ZO-1 and αPKCζ in XEGs at 96 h (immunostaining of cryosections). Scale bar: 50 µm. **e,** Live-cell imaging of SOX1 expression in a gastruloid (top panel, scale bar: 20 µm) and an XEG (lower panel, scale bar: 50 µm), grown with *Sox1*-GFP mESCs (see

Supplementary Videos 3-8). In all images, a single z-plane is shown. The arrows indicate epithelial structures. **b, d,** Cell nuclei were stained with DAPI.

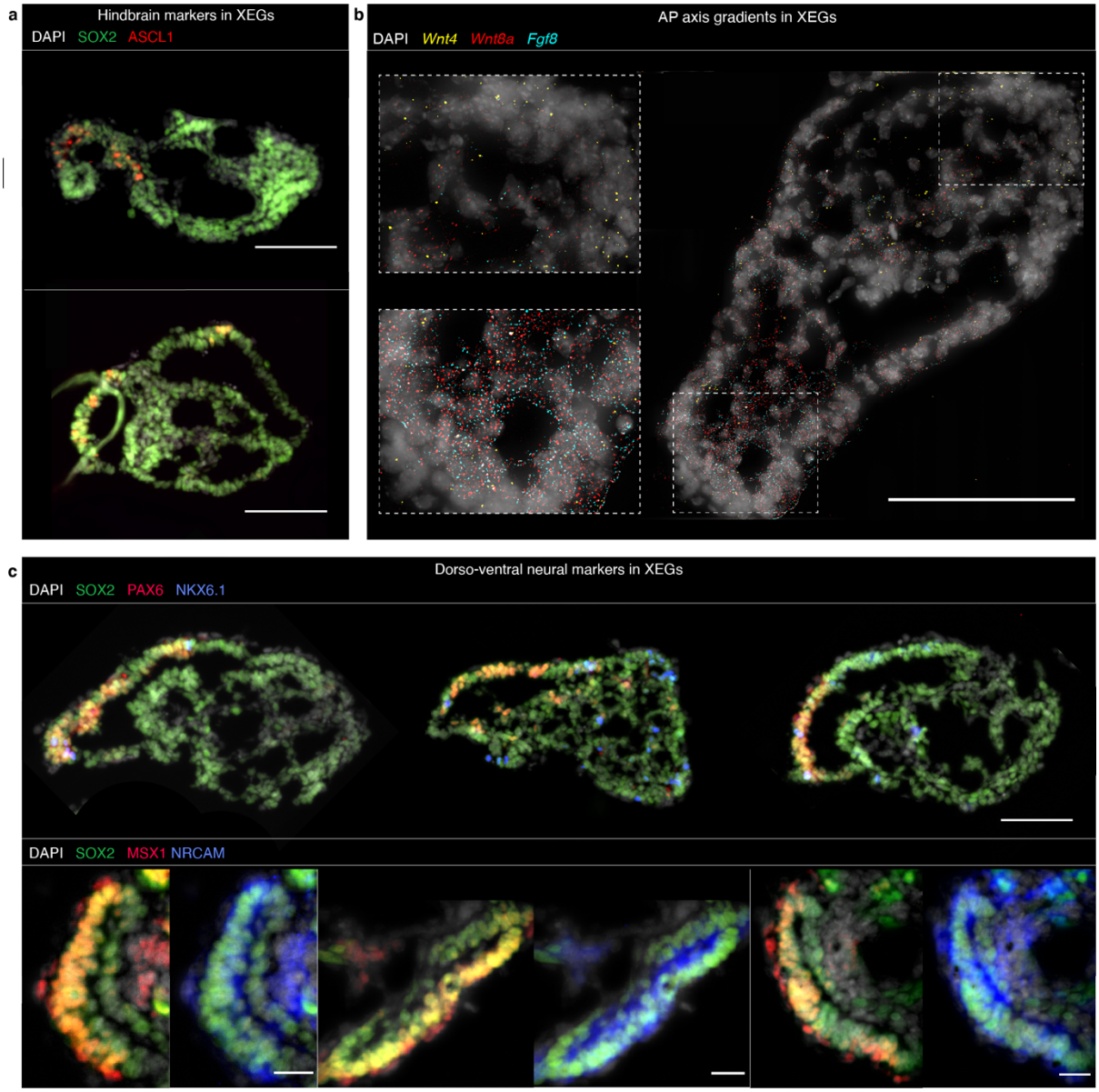

Fig. 2 | Neuroepithelia in XEGs show partial anteroposterior and dorsoventral patterning. a, Expression of SOX2 and ASLC1 in 96 h XEGs (immunostaining of sections). Scale bar: 100 µm. **b**, *Wnt4*, *Wnt8a* and *Fgf8* expression in XEGs at 96 h, visualized by smFISH on sections. Each diffraction limited dot is a single mRNA molecule. Scale bar: 100 µm. **c**, Expression of dorsal (PAX6, MSX1) and ventral (NKX6.1, NRCAM) neural tube markers in 96 h XEGs (immunostaining of sections). Top, expression of PAX6 and NKX6.1 Scale bar: 100 µm. Bottom, zoomed pictures of neural epithelia showing the expression of MSX1 and NRCAM. Scale bars: 20 µm. **a-c**, Cell nuclei were stained with DAPI.

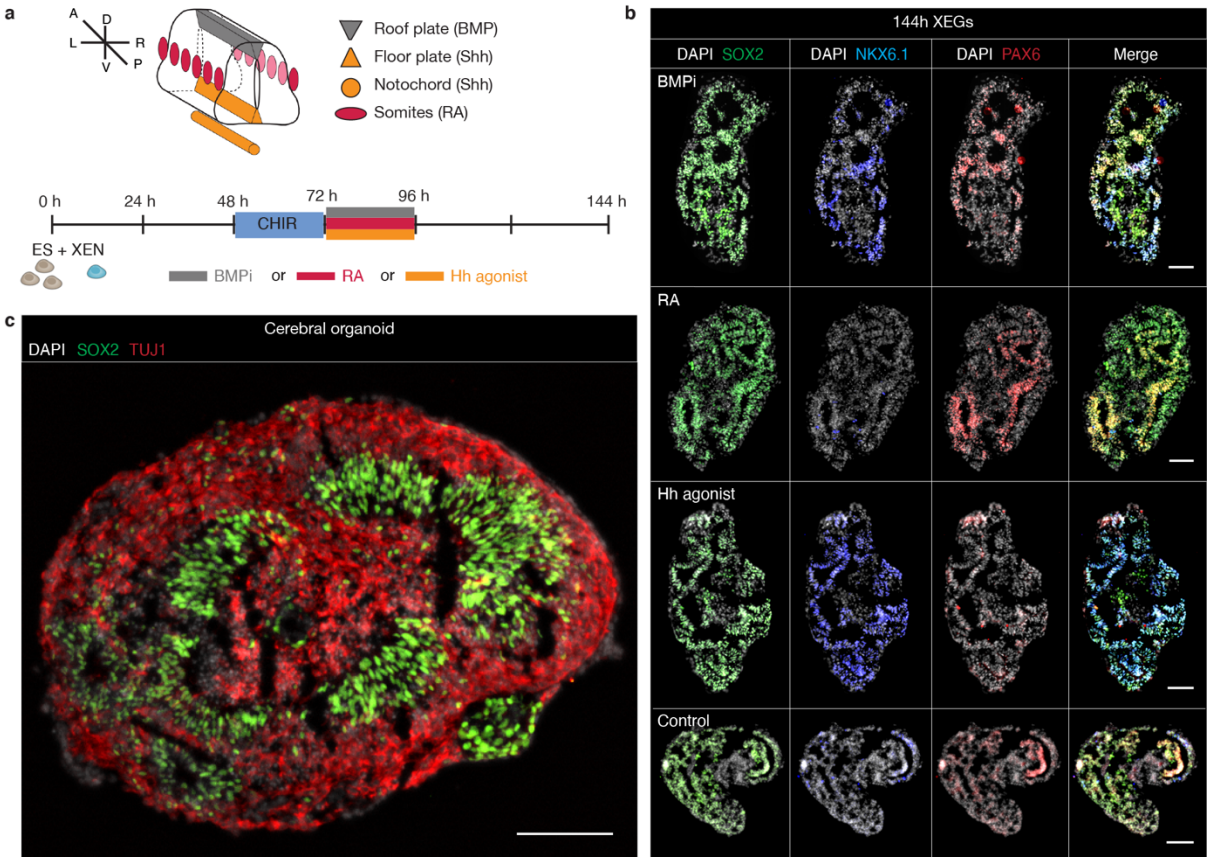

Fig. 3 | Signaling perturbation experiments and continued differentiation confirm neural character. a, Top: schematic of signaling sources patterning the developing neural tube *in vivo*. A: anterior, P: posterior, D: dorsal, V: ventral, L: left, R: right. Bottom: time line of the signaling experiments. XEGs were treated from 72 h to 96 h, with either BMP pathway inhibitor (BMPi), retinoic acid (RA) or hedgehog pathway agonist (Hh agonist). The XEGs were then allowed to grow for an additional 48 h before staining. **b,** Expression of SOX2, NKX6.1 and PAX6 in XEGs at 144 h, treated with the indicated factors (immunostaining of sections). n = 3 experiments. Scale bars: 100 µm. **c,** Expression of SOX2 and TUJ1 in XEGs, 8 days after cell seeding, differentiated according to a cerebral organoid protocol for 4 days (immunostaining of sections). Scale bar: 100 µm. **b-c**, Cell nuclei are stained with DAPI.

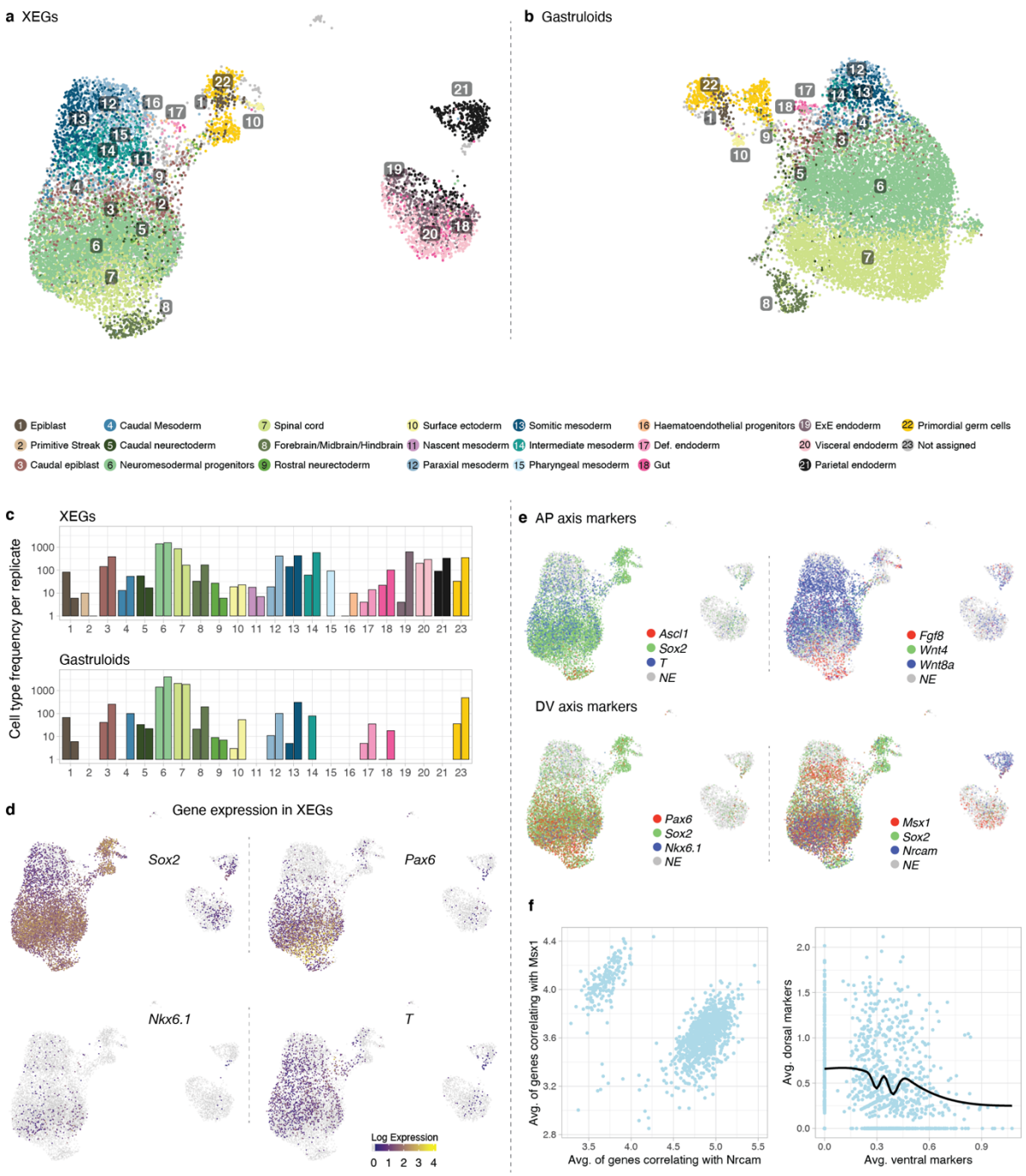

Fig. 4 | Single-cell RNA-seq reveals the transcriptional profiles of XEG cells. a,**b**, UMAP of cells in XEGs and gastruloids colored by cell type based on the mapping to *in vivo* data shown in Supplementary Fig. 4a,b. **c**, Cell type frequencies for both replicates in XEGs and gastruloids. **d**, *Sox2*, *Pax6*, *Nkx6.1* and *T* log-expression levels indicated by color in UMAPs of XEGs. **e**, Top, UMAP of cells in XEGs with log expression of genes expressed along the anteroposterior (AP) axis indicated by colors. Left: *Aslc1*, *Sox2* and *T*, right: *Wnt4*, *Wnt8a* and

Fgf8. Bottom, UMAP of cells in XEGs with log expression of genes expressed along the dorsoventral (DV) axis indicated by colors. Left: *Pax6*, *Sox2* and *Nkx6.1*, right: *Msx1*, *Sox2* and *Nrcam* indicated by color. All UMAPs show both replicates, batch corrected. **f**, Left, scatter plot of the average expression of the top 10 genes correlating most strongly with *Msx1* and *Nrcam*, respectively, in our scRNA-seq data. Right, scatter plot of the average expression of 10 canonical marker genes for dorsal and ventral neural progenitors, respectively, with the moving average indicated by the black solid line (see Methods for the gene lists).

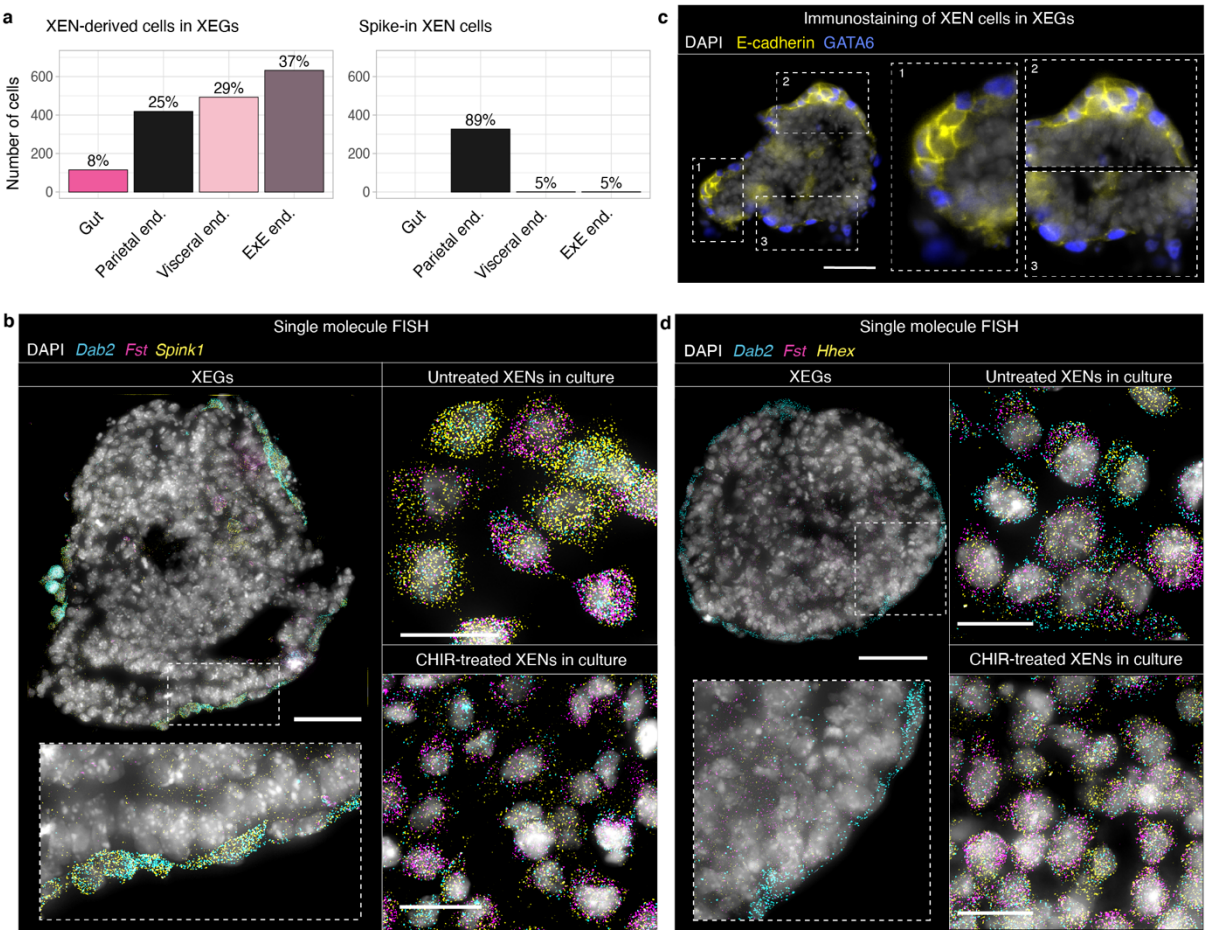

Fig. 5 | Most XEN cells become VE-like in XEGs. a, Left, cell types of XEN-derived cells in XEGs. Cells were classified as gut, PE ("parietal end."), embryonic VE ("visceral end.") or extraembryonic VE ("ExE end.") by mapping to the data set from the Pijuan-Sala et al. dataset[36]. Right, cell types of spiked-in XEN cells. **b**, *Dab2*, *Spink1* and *Fst* expression in a section of an XEG at 96 h (left, scale bar: 50 µm), in XEN cells cultured under standard maintenance conditions (top right, scale bar: 20 µm) and in XEN cells treated with CHIR according to the XEG protocol (bottom right, scale bar: 20 µm). Expression was visualized by smFISH. Each diffraction limited dot is a single mRNA molecule. **c**, Expression of E-cadherin in XEGs at 96 h (immunostaining of sections). XEN cells were localized by expression of GATA6. Scale bars: 50 µm. **d**, *Dab2*, *Fst* and *Hhex* expression in a section of an XEG at 96 h (left, scale bar: 50 µm), in XEN cells cultured under standard maintenance conditions (top right, scale bar: 20 µm) and in XEN cells treated with CHIR according to the XEG protocol

(bottom right, scale bar: 20 μm). Expression was visualized by smFISH. Each diffraction limited dot is a single mRNA molecule. **b-d**, Cell nuclei were stained with DAPI. The dashed boxes are shown at a higher magnification in the insets.

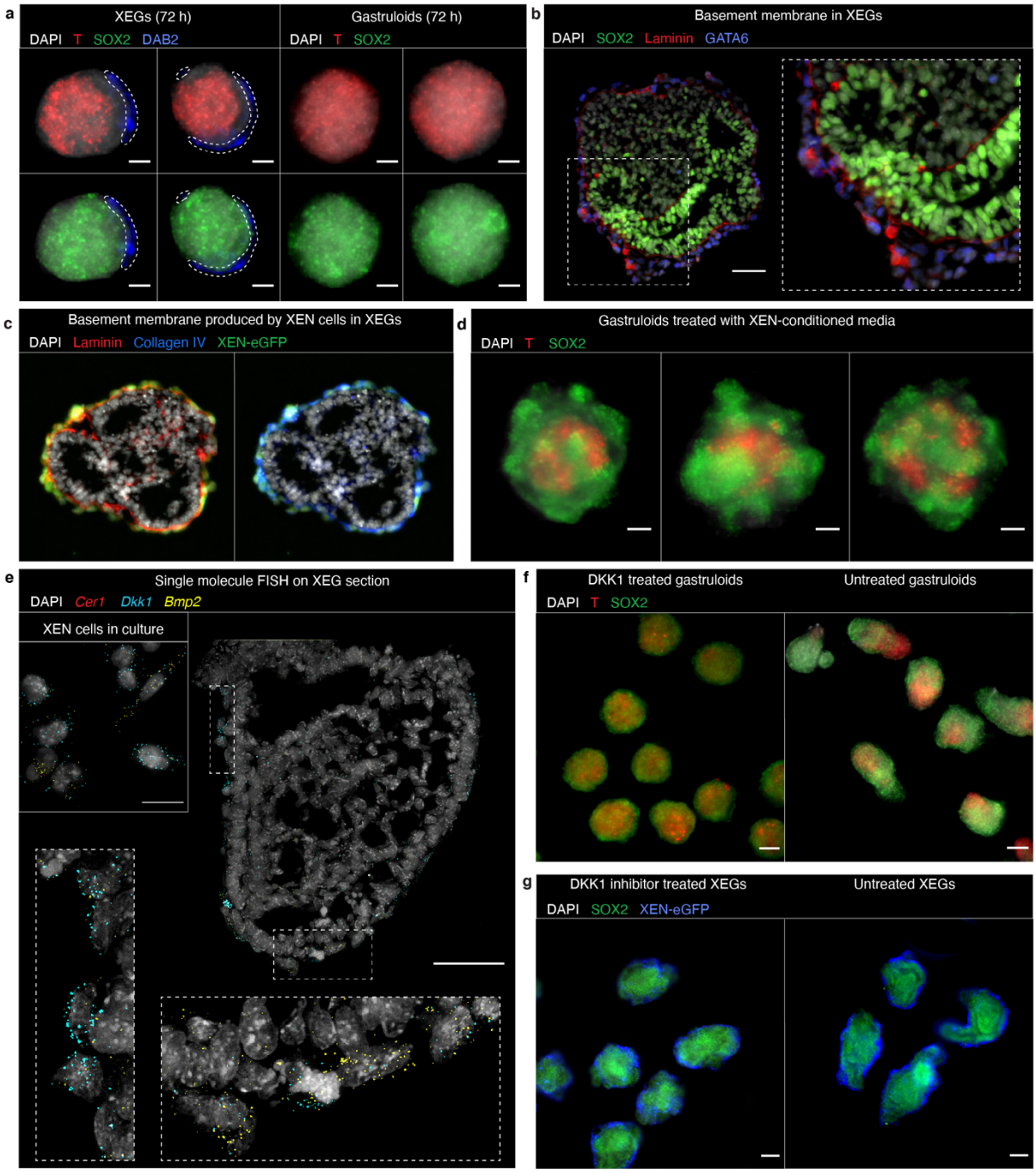

Fig. 6 | XEN cells guide symmetry breaking by locally inhibiting primitive streak formation. a, T and SOX2 expression in XEGs (left) and gastruloids (right) at 72 h (z-projection of whole mount immunostaining). XEN cells were localized by expression of DAB2 and are indicated by a dashed outline. **b**, Expression of SOX2 and laminin in XEGs at 96 h (immunostaining of sections). XEN cells were localized by expression of GATA6. The dashed boxes are shown at a higher magnification in the insets. Scale bars: 50 µm. **c**, Expression of

collagen IV and laminin in XEGs at 96 h (immunostaining of sections). XEN cells were localized by expression of H2B-GFP. Scale bars: 100 µm. **d**, T and SOX2 expression in gastruloids grown in XEN-conditioned media at 96 h (z-projection of whole mount immunostaining). **e**, *Cer1*, *Dkk1* and *Bmp2* expression in a section of a XEG at 96 h (scale bar: 50 µm) or XEN cells cultured under standard maintenance conditions (inset, scale bars: 20 µm). Expression was visualized by smFISH. Each diffraction limited dot is a single mRNA molecule. **f**, T and SOX2 expression in 96 h gastruloids treated with 200 ng/mL DKK1 and untreated (z-projection of whole mount immunostaining). Scale bars: 100 µm. **g**, T and SOX2 expression in 96 h XEGs treated with 0.25 µM DKK1 inhibitor WAY-262611 and untreated (z-projection of whole mount immunostaining). Scale bars: 100 µm. **a-g**, Cell nuclei were stained with DAPI.

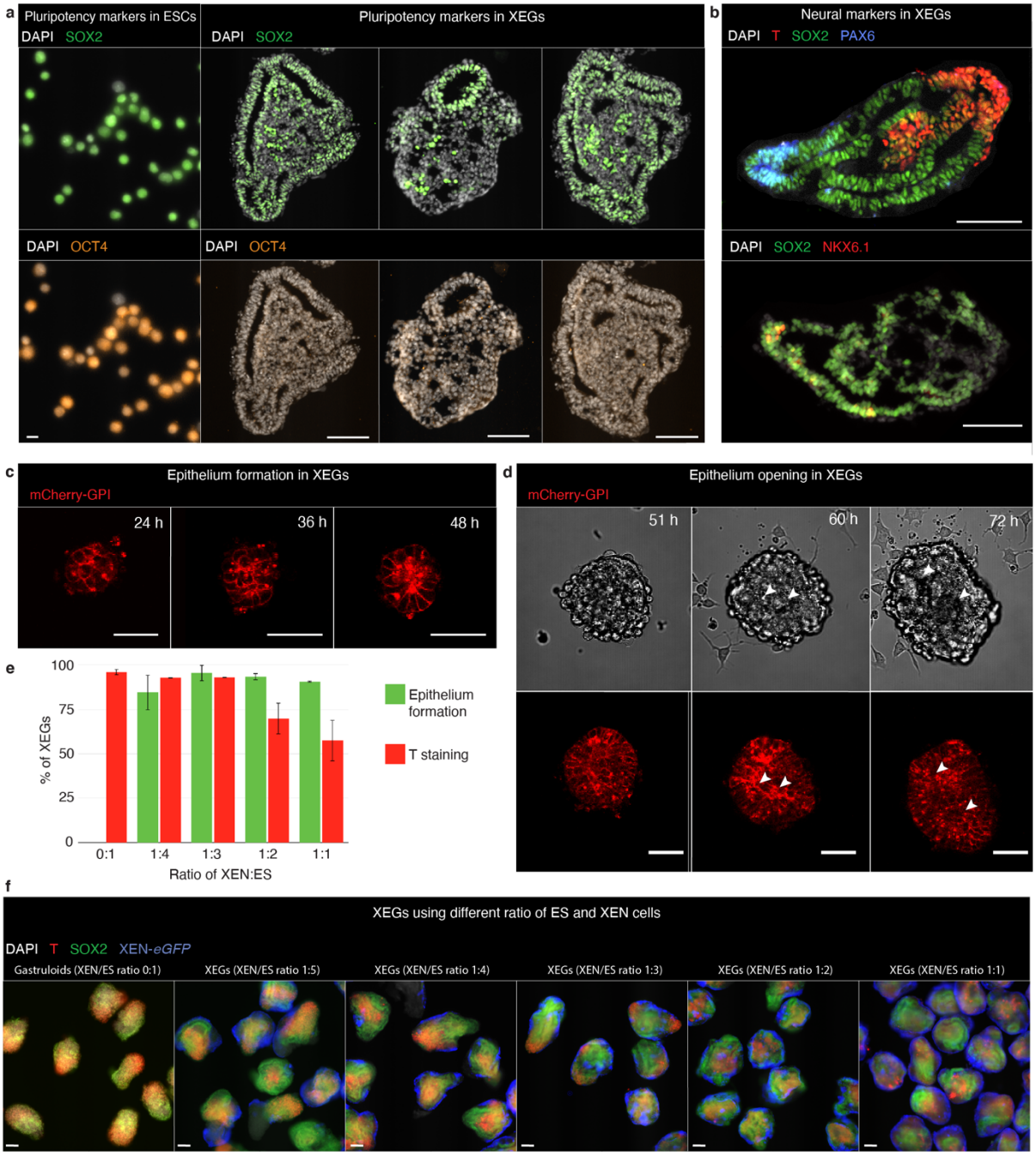

Supplementary Fig. 1 | Optimization and characterization of XEGs. a, Expression of SOX2 and OCT4 (immunostaining) in sections of XEGs at 96 h (left, scale bars: 100 µm) and cultured ESCs (right, scale bars: 10 µm). **b**, Expression of T, SOX2, PAX6, MASH1 and NKX6.1 (immunostaining) in 96 h XEGs. Scale bars: 100 µm. **c-d,** Live-cell imaging of morphological changes in XEGs grown from mCherry-GPI expressing mESCs. mCherry-GPI is localized to the cell membrane. In all images, a single z-plane is shown. **c**, Rosette formation. The center of the rosette is indicated by a dashed line. Inset: tracing of cell outlines. **d**,

Cavitation of rosettes. Dashed lines indicate the opening cavities. The top row shows the brightfield channel, the bottom row shows the mCherry channel. See also Supplementary Videos 1 and 2. Scale bars: 50 µm. **e**, Average fraction of aggregates showing epithelial structures and T staining at 96 h for different starting ratios of ESCs and XEN cells (n = 2 experiments, error bars show standard deviation). **f**, SOX2 (neural progenitors-like cells) and T (primitive streak-like cells) expression in gastruloids and XEGs with different starting ratios of ESCs and XEN cells (z-projection of whole mount immunostaining). Scale bars: 100 µm. **a, b, f,** Cell nuclei were stained with DAPI.

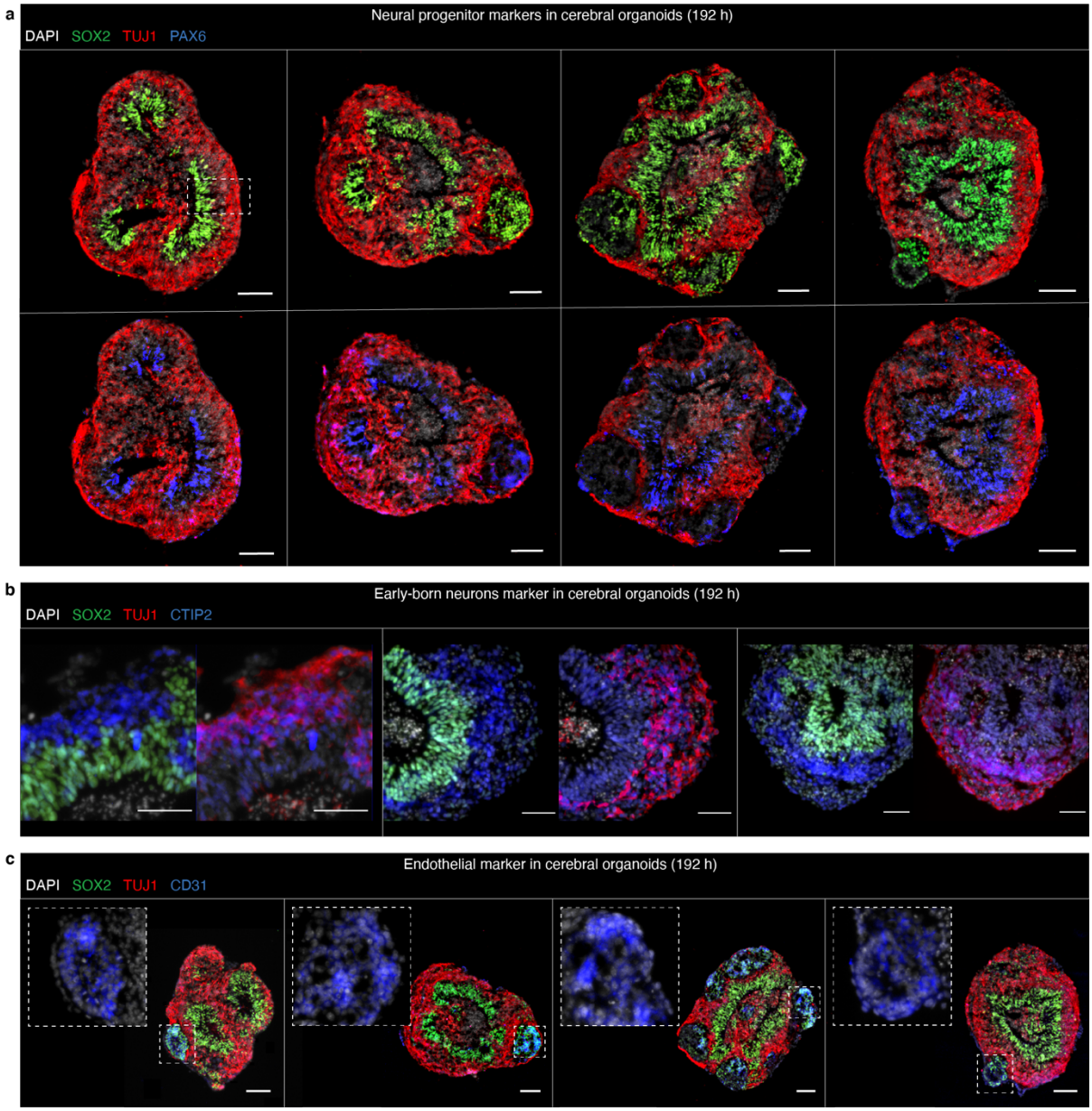

Supplementary Fig. 2 | Developing brain markers are expressed in XEGs further differentiated with a cerebral organoid protocol. a, b, c, Immunostaining in sections of XEGs on day 8 after cell seeding. **a**, TUJ1, SOX2 (top) and PAX6 (bottom). The dashed box highlights an example of layered organization adjacent to a ventricle-like cavity. **b,** TUJ1, SOX2 and CTIP2, a marker for early-born neurons. **c,** TUJ1, SOX2 and CD31. Insets show clusters of cells positive for the endothelial marker CD31. Cell nuclei were stained with DAPI. Scale bars: 100 µm.

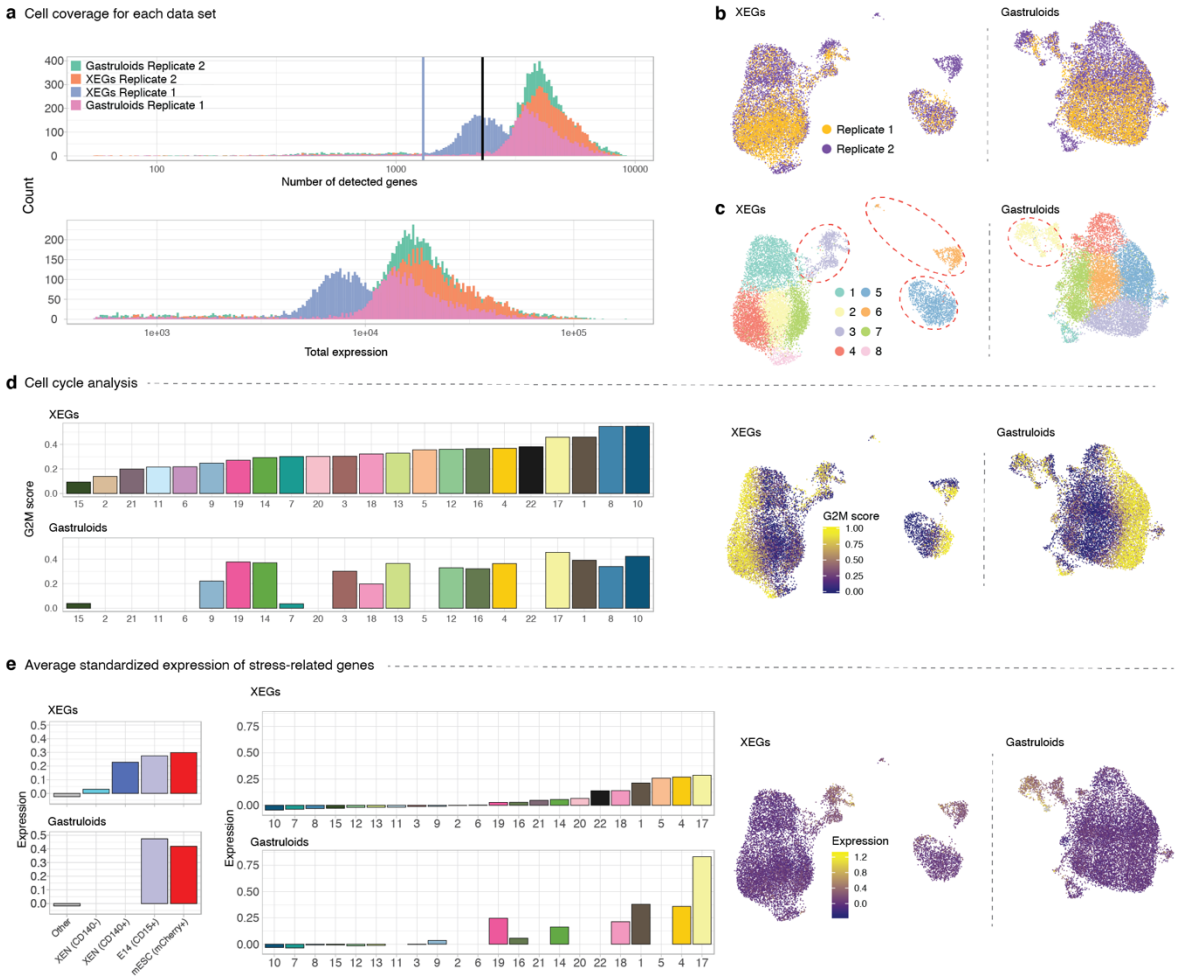

Supplementary Fig. 3 | Quality control of single-cell RNA-seq data. a, Top, number of detected genes per cell in each replicate; the blue line indicates a quality control threshold for XEGs from replicate 1 and the black line for the remaining datasets. Bottom, total expression per cell for each dataset. **b**, UMAP of cells in XEGs and gastruloids, colored by replicate. **c**, UMAP of cells in XEGs and gastruloids, colored by Louvain clustering. The encircled clusters contain the spiked-in cells. **d**, Left, average G2M scores for each cell type. Right, UMAPs of cells in XEGs and gastruloids colored by G2M score. **e**, Left, average standardized expression of stress-related genes in spike-in cells. Middle, expression of stress-related genes by cell type. Right, UMAPs of cells in XEGs and gastruloids with expression of stress-related genes indicated by color. **b-e**, UMAPs contain both replicates, batch corrected.

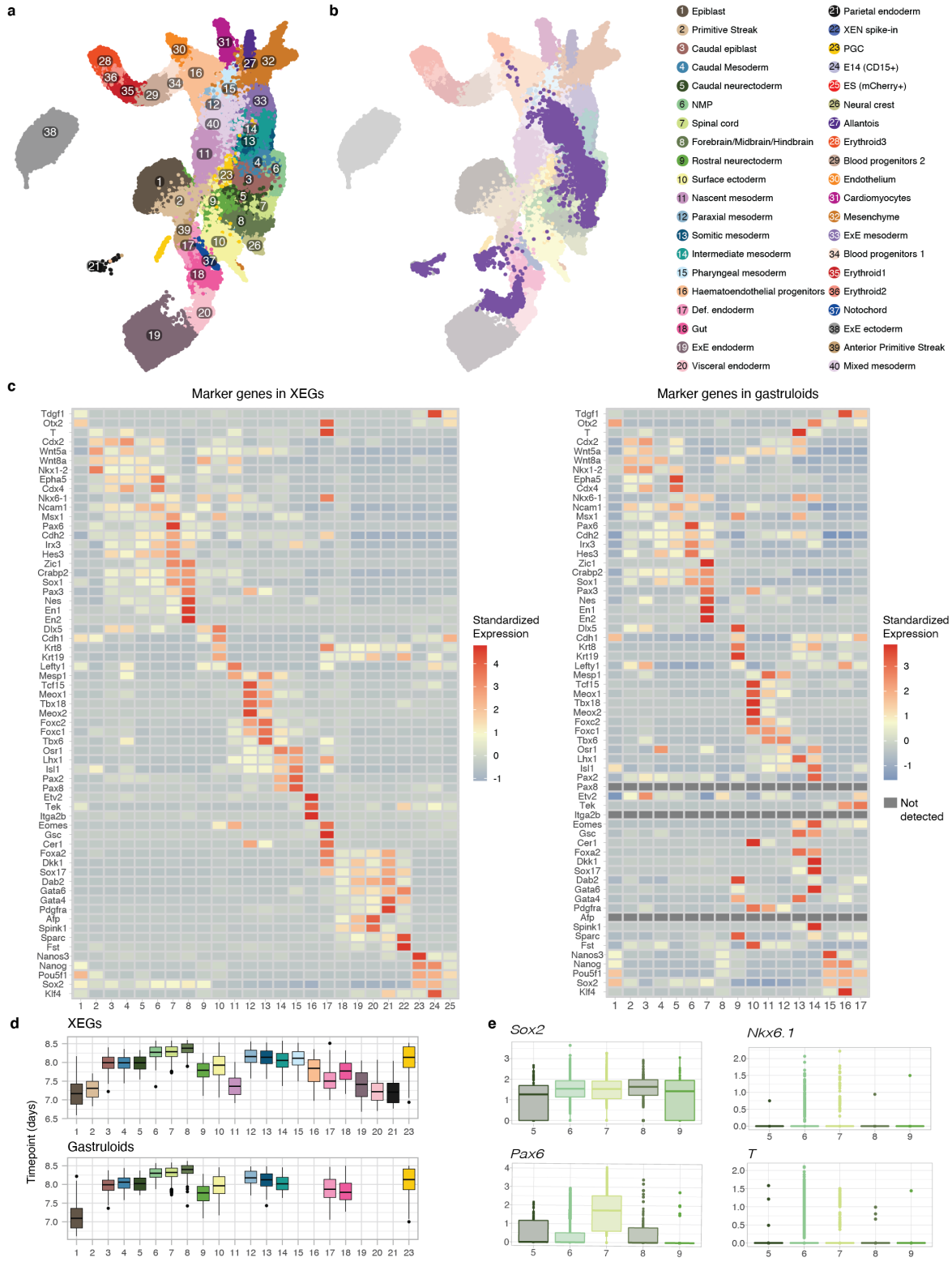

Supplementary Fig. 4 | Single-cell RNA-seq resolves cell type diversity in XEGs and gastruloids. a, UMAP of the Pijuan-Sala et al.[36] dataset with cell types indicated by color. **b**, MNN mapping of XEG cells from replicate 2 (bright colors) to the Pijuan-Sala et al. dataset

(dim colors), as an example for the mapping procedure. **c**, Heat map of standardized expression of genes associated with mouse embryonic development in XEGs and gastruloids. References describing the *in vivo* expression of the genes are given in Supplementary Table 1. **d**, Developmental age of cell types based on mapping to *in vivo* data. **e**, Expression of *Sox2*, *Pax6* and *Nkx6.1* and *T* in XEGs, as measured by single-cell RNA-seq.

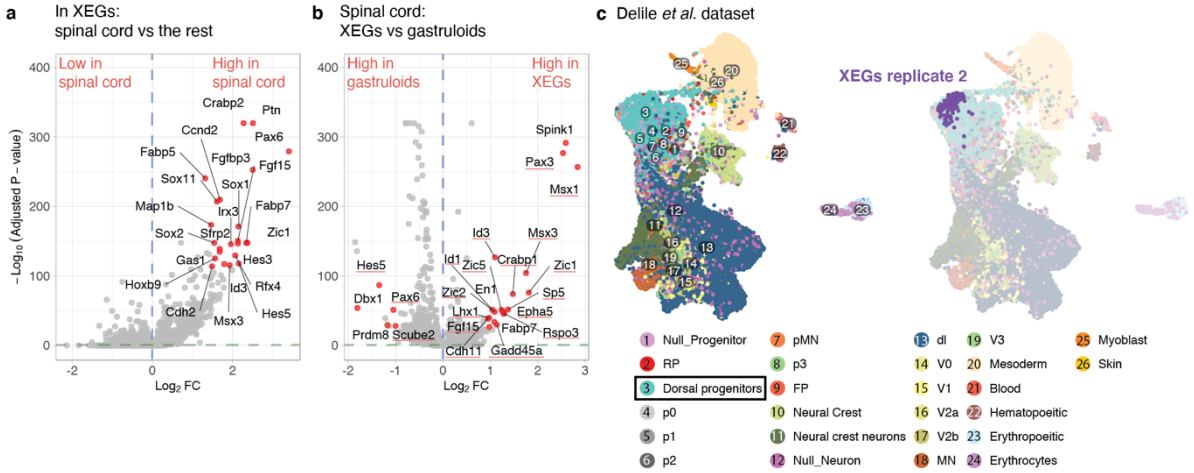

Supplementary Fig. 5 | Neuroepithelial cells are biased towards a dorsal expression profile. a, Gene expression differences between cells classified as "spinal cord" and all other cells in XEGs (fold-change vs p-value). Named genes are expressed in the neural tube according to previous studies (Supplementary Table 2). **b**, Gene expression differences between cells classified as "spinal cord" in gastruloids and XEGs (fold-change vs p-value). Underlined genes are expressed in the dorsal part of the neural tube according to previous studies (Supplementary Table 4). **c**, Left, UMAP of the cells in the Delile et al. dataset[37], colored by cell type. Right, MNN mapping of cells classified as "spinal cord" in replicate 2 XEGs (bright colors) to the Delile et al. dataset (dim colors), as an example of the mapping procedure.

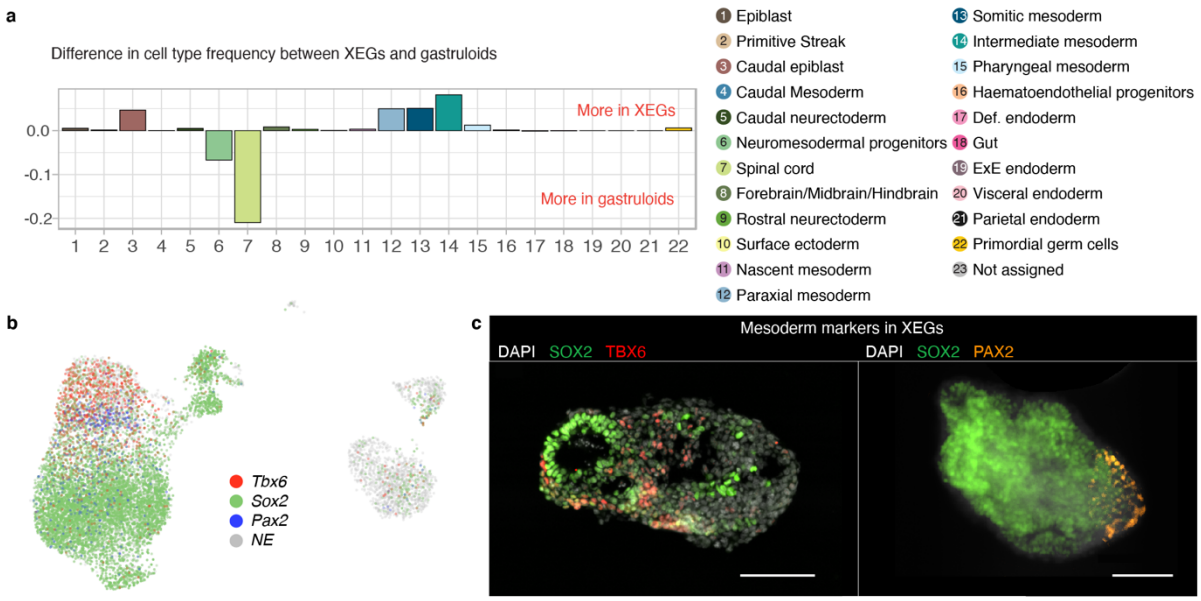

Supplementary Fig. 6 | XEGs and gastruloids differ in cell type distribution. a, Differences between relative frequencies of cell types in XEGs and gastruloids. **b,** UMAP of cells in XEGs (both replicates, batch corrected) with log expression of *Tbx6*, *Sox2* and *Pax2* indicated by color. **c,** Expression of mesoderm markers. Left, TBX6 expression in a 96 h XEG (immunostaining of a section). Right, PAX2 expression in a 96 h XEG (wholemount immunostaining). Scale bars: 100 µm. Nuclei were stained with DAPI.

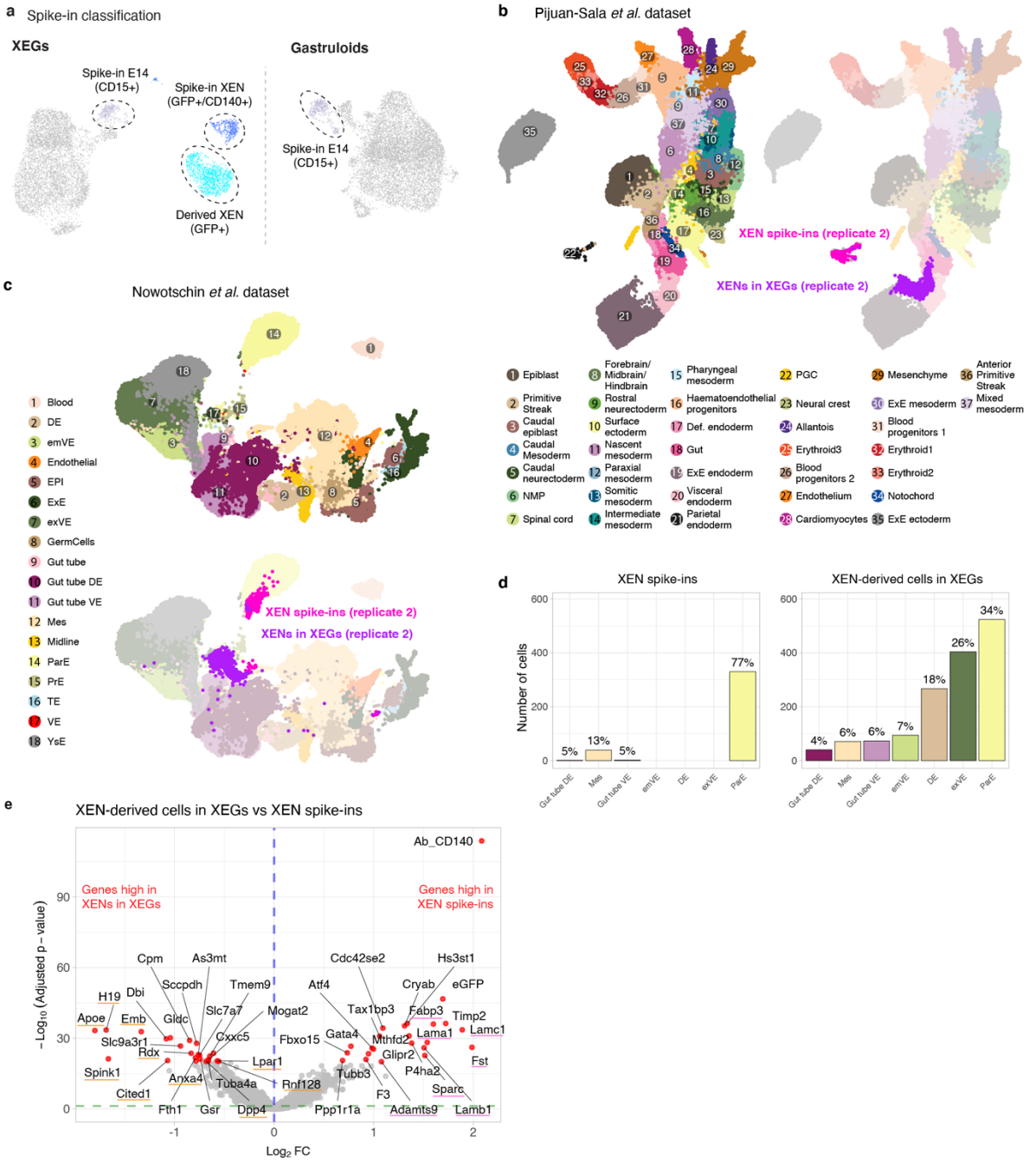

Supplementary Fig. 7 | Most XEN-derived cells are visceral endoderm-like in XEGs. a, UMAP of cells in XEGs and gastruloids with spike-in cells and XEN derived cells highlighted by color and circled (replicate 2). **b**, **c**, UMAPs of the Pijuan-Sala[36] or Nowotschin[41] dataset, respectively. XEN spike-ins and XEN-derived cells from XEGs replicate 2 (bright colors) are mapped to the *in vivo* datasets (dim colors). **d**, Cell type frequencies of XEN spike-ins and XEN derived cells in XEGs, resulting from knn assignments based on the mapping in **(c)**. **e**,

Gene expression differences between XEN spike-ins and XEN-derived cells in XEGs (fold-change vs p-value). Orange and pink lines indicate genes with PE-like and VE-like identity, respectively (see Supplementary Table 3). DE: definitive endoderm, emVE: embryonic visceral endoderm, EPI: epiblast, ExE: extraembryonic ectoderm, exVE: extraembryonic visceral endoderm, Mes: mesoderm, ParE: parietal endoderm, PrE: primitive endoderm, TE: trophectoderm, VE: visceral endoderm, YsE: yolk sac endoderm.

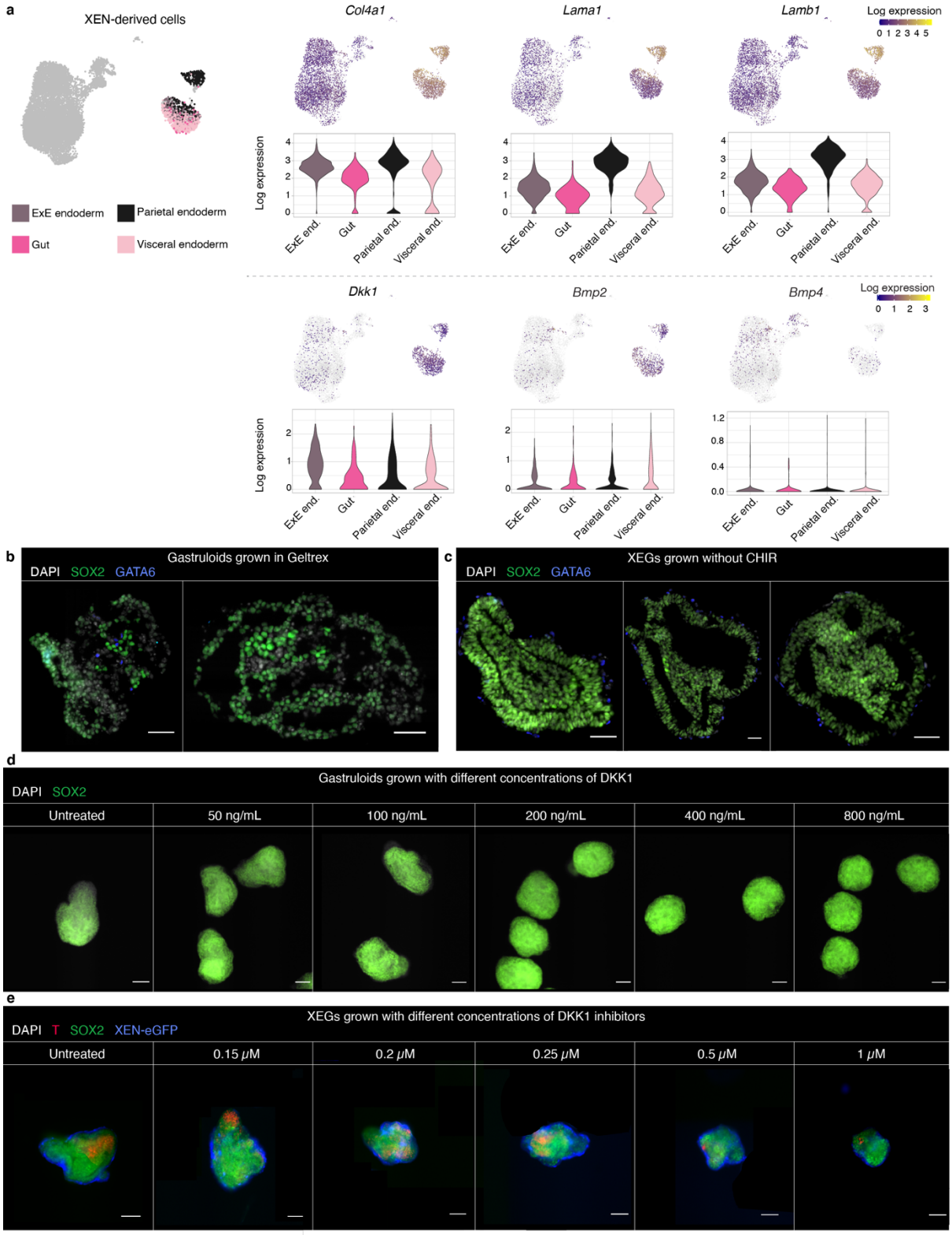

Supplementary Fig. 8 | Basement membrane components and the WNT inhibitor DKK1, all expressed exclusively by XEN cells, play a role in epithelia formation. **a**, Expression of genes in XEN-derived cells. Left, UMAP of cells in XEGs with XEN-derived cells colored by

cell type (gut, parietal endoderm (parietal end.), embryonic VE (visceral end.) or extraembryonic VE (ExE end.)). Top-right, expression of basement membrane components collagen IV *(Col4a1)*, laminin alpha 1 (*Lama1*) and laminin beta 1 (*Lamb1*). Bottom-right, expression of signaling factors DKK1 (*Dkk1*), BMP2 (*Bmp2*) and BMP4 (*Bmp4*). UMAPs indicate log expression by color and contain both replicates, batch corrected. A violin plot of log expression in XEN-derived cell types is shown below the UMAP for each gene. **b**, Expression of SOX2 and GATA6 in gastruloids grown in Geltrex at 96 h (immunostaining of crysections). Scale bars: 50 µm. **c**, Expression of SOX2 in XEGs grown without CHIR (immunostaining of cryosections). No specific T staining could be detected (data not shown). XEN cells were localized by expression of GATA6. Scale bars: 50 µm. **d**, Expression of SOX2 in 96 h gastruloids treated with various concentrations of DKK1 between 24 h and 96 h (wholemount immunostaining). Scale bars: 100 µm. **e**, Expression of SOX2 and T in 96 h XEGs treated with various concentrations of DKK1 inhibitor WAY-262611 between 24 h and 96 h (wholemount immunostaining). XEN cells were localized by endogenous expression of H2B-GFP. Scale bars: 100 µm. **b-e**, Cell nuclei were stained with DAPI.

Supplementary Table 1 | Marker genes used for cell type annotation in the single-cell RNA-seq data

Genes	Expressing cell types in our data	Other expressing cell types not found in our data	References
Nanog	Pluripotency Germ cells		Chambers et al., 2003, *Cell* Chambers et al., 2007, *Nature*
Nanos3	Germ cells		Tsuda et al., 2003, *Science*
Otx2	Early epiblast PGCs	Anterior epiblast Forebrain/midbrain VE/AVE	Acampora et al., 2009, *Mech Dev* Chu, G. C., et al., 2004, *Development* Zhang, J., et al., 2018, *Nature*
Oct4	mESC Epiblast PGCs		Pesce, M., & Schöler, H. R. 2000. *Molecular Reproduction and Development* Shi and Jin, 2010, *Stem Cell Res. Ther.* Iwafuchi-Doi, M., et al. 2012. *Development*
Tcf15	Paraxial mesoderm Presomitic mesoderm	ICM Epiblast	Davies et al., 2013, *Cell Rep* Burgess, R., et al. 1995, *Developmental Biology*
Sox2	mESC Caudal epiblast NMPs Neural progenitors PGCs		Henrique et al., 2015, *Development*
T	Primitive streak Caudal epiblast Nascent mesoderm Caudal mesoderm NMPs		Henrique et al., 2015, *Development* Sadahiro, T., et al. 2018. *Cell Stem Cell* Edri, S., Hayward, P., Jawaid, W., & Martinez Arias, A. 2019. *Development*
Nkx1-2	Caudal epiblast NMPs		Henrique et al., 2015, *Development* Edri, S., Hayward, P., Jawaid, W., & Martinez Arias, A. 2019. *Development*
Fst	Caudal epiblast turned off after Presomitic mesoderm Somites Parietal endoderm		Cunningham et al., 2016, *Biol. Open* Feijen, A., et al., 1994, *Development* Ribes, V., et al., 2009, *Development*
Tbx6	Caudal mesoderm Paraxial mesoderm		White et al., 2003, *Development* Chalamalasetty et al., 2014, *Development*
Meox1	Presomitic mesoderm Somites		Jukkola et al., 2005, *Genesis* Candia, A. F., et al., 1992. *Development*
Etv2	Heamatoendothelial progenitors		Gong, W., et al., 2017. *Nature Communications*
Tek Tie2	Heamatoendothelial progenitors		Gong, W., et al., 2017. *Nature Communications*
Itga2b Cd41	Heamatoendothelial progenitors		Gong, W., et al., 2017. *Nature Communications*
Dlx5	Rostral neuroectoderm Surface ectoderm?		Yang, L., et al., 1998. *The Journal of Neuroscience*
Osr1	Intermediate mesoderm Pharyngeal mesoderm		Wang et al., 2005. *Dev. Biol.* Francou, A., et al., 2013. *Biochimica Et Biophysica Acta*
Msx1	Caudal epiblast Neural tube Surface ectoderm	Embryonic and extra-embryonic mesoderm VE Developing gut	Nowotschin, S., et al. 2019. *Nature* Sun, J., et al. 2016. *Dev. Biol.* Houzelstein, D., et al., 2000. *Development*
Sparc	Parietal endoderm Visceral endoderm low		Holland, P. W., et al., 1987. *The Journal of Cell Biology*
Pax6	Neuroepithelium Forebrain/Midbrain/Hindbrain		Bel-Vialar et al., 2007. *Dev. Biol.* Kayam, G., et al. 2013. *Development* Jessell, T. M. 2000. *Nature Reviews Genetics*
Pax3	Neural tube Somites Brain		Goulding, M. D., et al., 1991. *The EMBO Journal* Mansouri, A., et al., 2001. *Development*
Sox1	Neural plate Neural tube Developing brain		Pevny et al., 1998. *Development* Wood and Episkopou, 1999. *Mech. Dev.*
Wnt8a	Caudal epiblast		Cunningham et al., 2015. *Dev. Dyn.* Parr Brian A. et al., 1993. *Development*
Wnt5a	Caudal epiblast		Yamaguchi et al., 1999. *Development*
Foxa2	Caudal epiblast Extraembryonic tissue Developing gut		Kojima et al., 2014. *Cell Stem Cell* Lu and Robertson, 2004. *Dev. Biol.* Nowotschin, S., et al. 2019. *Nature*

Supplementary Table 2 | Genes differentially expressed between spinal cord-like cells and the other cells types in XEGs.

Gene	Log FC	p.adjust	Reference
Ccnd2	1.684190185	1.37E-210	Lacomme, M., et al., (2012). *Molecular and Cellular Biology*
Crabp2	2.27328271	0	Ruberte, E., et al., (1992). *Development*
Id3	1.789970808	5.65E-118	Wine-Lee, L., et al., (2004). *Development*
Fabp7 (BLBP)	2.339513279	2.65E-148	Feng, L., Hatten, M. E., & Heintz, N. (1994). *Neuron*
Rfx4	2.066843727	3.40E-130	Ashique, A. M., et al. (2009). *Science Signaling*
Hoxb9	1.561341789	4.07E-126	Graham, A., Maden, M., & Krumlauf, R. (1991). *Development*
Cdh2	1.486458795	1.15E-114	Radice, G. L., et al., (1997). *Developmental Biology*
Msx3	1.925035016	3.06E-116	Misra, K., Luo, H., Li, S., Matise, M., & Xiang, M. (2014). *Development*
Pax6	3.403368474	4.04E-280	Jeong, J., & McMahon, A. P. (2005). *Development*
Fabp5	1.316127675	1.97E-241	Shimamoto, C., et al. (2014). *Human Molecular Genetics*
Sfrp2	1.677002264	9.74E-140	Misra, K., & Matise, M. P. (2010). *Developmental Biology*
Hes3	2.132129411	2.12E-147	Lobe, C. G. (1997). *Mechanisms of Development*
Ptn	2.50622717	0	Magdaleno, S., et al. (2006). *PLoS Biology*
Fgf15	2.131102328	2.17E-151	McWhirter, J. R., et al., (1997). *Development*
Irx3	1.957663655	1.71E-146	Lebel, M., et al. (2003). *Molecular and Cellular Biology*
Zic1	2.371434543	1.56E-148	Nagai, T., et al., (1997). *Developmental Biology*
Fgfbp3	2.502793725	1.10E-253	Yu, K., McGlynn, S., & Matise, M. P. (2013). *Development*
Hes5	2.152139781	9.35E-119	Hatakeyama, J., et al., (2004). *Development*
Map1b	1.46443751	3.03E-174	Fawcett, J. W., et al., (1994). *Neuroscience*
Gas1	1.676359071	1.03E-135	Allen, B. L., Tenzen, T., & McMahon, A. P. (2007). *Genes & Development*
Sox11	1.610646468	6.85E-208	Tanaka, S., et al., (2004). *Molecular and Cellular Biology*
Sox2	1.54213575	1.78E-148	Hoffmann, S. A., et al., (2014). *Development*
Sox1	2.143957789	5.90E-172	Hoffmann, S. A., et al., (2014). *Development*

Supplementary Table 3 | Genes differentially expressed between XEN-derived cells in XEGs and cultured XEN cells.

Gene	Log FC	Expression summary	Reference
Apoe	-1.80	VE > PE	Basheeruddin, K., et al., (1987)
H19	-1.69	VE > PE	Long, L., & Spear, B. T. (2004).
Spink1	-1.66	VE	Goh, H. N., et al. (2014).
Emb	-1.33	pan-endoderm	Brown, K., et al., (2010).
Cited1 (Mgs1)	-1.07	exVE	Dunwoodie, S. L., et al., (1998).
Rdx (Radixin)	-0.83	VE	Igarashi, H., et al. (2018). McClatchey, A. I., et al.,(1997).
Anxa4	-0.78	pan-endoderm	Brown, K., et al., (2010).
Dpp4	-0.68	VE	Sherwood, R. I., et al. (2007).
Lapr1 (Lpa1)	-0.57	VE	Koike, S., et al., (2009).
Rnf128 (Greul)	-0.56	VE	Borchers, A. G. M., et al., (2002).
Gata4	0.77	pan-endoderm	Morrisey, E. E., et al.,(1998).
P4ha2	0.79	PrE	Ohnishi, Y., et al. (2014).
Adamts9	1.08	PE	Jungers, K. A., et al., (2005).
Lamb1	1.51	PE	Miner, J. H., et al., (2004).
Sparc	1.51	PE	Mason, I. J., et al., (1986).
Lama1	1.54	PE	Hogan, B. L., et al., (1980).
Fabp3	1.60	exVE - PE	Cheng, S., et al. (2019). Futaki, S., et al. (2003).
Lamc1	1.89	PE	Smyth, N., et al., (1999).
Fst	1.99	PE	Feijen, A., et al. (1994).

Supplementary Table 4 | Genes differentially expressed between spinal cord-like cells in XEGs and gastruloids.

Gene	Log FC	Expression summary	BMP signalling response	Reference
Msx1	2.84	Dorsal neural tube + small ventral domain	BMP (Lee, K. J., & Jessell, T. M. (1999))	Misra, K., et al., (2014). Duval, N., et al. (2014).
Spink1	2.59			
Pax3	2.53	Dorsal neural tube	BMP (Lee, K. J., & Jessell, T. M. (1999))	Kriks, S., et al., (2005).
Zic1	1.81	Dorsal neural tube	BMP (Lee, K. J., & Jessell, T. M. (1999))	Nagai, T., et al., (1997). Aruga, J.,et al., (2002).
Msx3	1.75	Dorsal neural tube	BMP4 (Shimeld, S. et al., (1996))	Misra, K., et al., (2014). Duval, N., et al. (2014).
Crabp1	1.47	Forebrain, Neural crest + dorsal neural tube	-	Ruberte, E., et al., (1991).
Sp5	1.37	Midbrain and dorsal neural tube	-	Andoniadou, C. L., et al. (2011). Dunty, W. C., et al., (2014).
Epha5	1.29	Dorsal and ventral	BMP2 (Yamada, T., et al., (2016))	Abdul-Aziz, N. M., et al., (2009). Ono, K., et al. (2014).
Rspo3	1.28	Forebrain, dorsal neural tube	-	Nam, J.-S., et al., (2007).
En1	1.27	Hinbrain/Midbrain Ventral neural tube	Not affected by BMP (Timmer, J. R., et al., (2002))	Ericson, J., et al. (1997). Sgaier, S. K., et al., (2007).
Zic5	1.23	Dorsal neural tube and head fold	BMP (Nakata, K., et a., (2000))	Inoue, T., et al., (2004).
Fabp7 (BLBP)	1.14	Ventral neural tube Midbrain	-	Delile, J., et al., (2019). Feng, L., et al., (1994).
Id3	1.10	The roof plate and dorsal neural ectoderm + small ventral domain	BMP (Wine-Lee, L., et al., (2004))	Wine-Lee, L., et al., (2004).
Zic2	1.09	Dorsal neural tube	BMP6/7 (Lee, K. J., & Jessell, T. M. (1999))	Ybot-Gonzalez, P., et al., (2007). Sanchez-Ferras, O., et al., (2014).
Gadd45a	1.08	Mostly dorsal neural tube Residual expression in ventral neural tube	BMP2 (Ijiri, K., et al. (2005))	Kaufmann, L. T., et al., (2011).
Id1	1.04	Roof plate and dorsal neural ectoderm + small ventral domain	BMP (Wine-Lee, L., et al., (2004))	Wine-Lee, L., et al., (2004).
Cdh11	0.98	Neural crest + dorsal neural tube	BMP7 (Awazu, M., et al., (2017))	Tondeleir, D., et al., (2014). Kashef, J., et al., (2009).
Lhx1	0.97	Dorsal interneurons	Not affected by BMP4/7 (Le Dréau, G., et al., (2012))	Le Dréau, G., et al., (2012).
Fgf15	0.95	Dorsal regions of the di-, mes and metencephalon	-	McWhirter, J. R., et al., (1997). Fischer, T., et al., (2011).

Supplementary Table 5 | Single-molecule FISH probes

Dab2	Hhex	Fst	Spink1
GTTTCTACTTCGTTAGACAT	TTCAGTCTTCTCCATTTAGC	AGTATTGTCGTTCACATCCT	CATTCTTCTGCTCCAATTCT
CAATGATTTTTATGCCAGAC	GTTGGTCTGTAGCAAAACAT	CGTTGAAAATCATCCACTTG	CAGGATTTCCATTCTTCCTT
GAGCAATGAAGGAAATCTTA	CAGTGCACCAAACATTTTCA	GGGGTTTATTCTTCTTGTTC	GTCTCTTCAGTAGTTCTGAA
CCTTTTTCTTATCTTCTTCC	CAACGCAATGCATGTTTGTT	TCTTTTTACATTTGCCCTGG	AATTAGCTGCATTCCTGACA
GGAGGTGGAAAGATATTATT	CTGGTATAGATACCGTATGT	TCTGTCTTATACAGGACCTG	CCAAATTCTTCCAGGAAAAG
GGAAGTCCTTAAACATTTCT	GAGGTCACATTTAGTCACTT	CCTGGACAAAAAACATCCCT	GGAAAATGTAACCTAGGTAG
CTTTGGTGGTTCATTAATCT	GCCTCCTAAAACTTAAAACC	CACAGTAGGCATTATTGGTC	GTGCCCTATAATAGGTATCT
GATTAGCTTGGCCTTGTATT	CTTAGGAAAGTCAGTCAAGA	CTCCATCATTTCCACAAAGG	TGCAAAAGCCAGAAGAACTA
CATCAGGCACATCATCAATA	AGTTGGGTATACCCTTTCAA	TAATCCAATGGATCTGCCCA	CACCTTAGCTGAAAAAGTGT
TCAATTACCCCAGTTTTCTC	GCAATGTAAGATGCCATGTA	CACAGGACTTTGTGATACAC	CAGAACACATTCATTGGCAT
CAAAAAATTGATGCTGGCCT	AAATGGCTTTGGAGTTAAGG	CAAGATCCAGAATGCTTCAC	TGCGTTTCCTGTTTTCAAAG
AAGATCGACGACTAATGGTT	GGCTGAGCAAAACAAGATTT	GATAGGAAAGCTGTAGTCCT	CTCTTTTAGGAAAGCCTTCC
GCTGAAGACAGCTTCAATTT	TCAAATGAGTCAGTTTCCCT	GCAACACTCTTCCTTGCTCA	AGAAGGGCAGAAAACTTTGG
CTGAGGAATGCCAACTTTAT	CTTACATTGAATTGTCCTGC	CCACGTTCTCACACGTTTCT	CTGAGAAGAAAGATGACAGC
AATCATCATGGTCTACATGC	GGCAGAGTTTTTACAAGAAG	CATTTTTTCCCAGGTCCGCA	ATCTTGACTTTCAGCAAGGC
TTCAACAGTTGATTGGCATC	CGTTCATCTGATGATGAATG	TCTTTGCATCTGGCCTTGAG	GGTAGCCATAACAGAGTTCA
ACACCATCACCTTTGAACCT	CTTTAGGTGTCATGTTTAGG	CTGTACTTCTAGTTCCGGCT	GAACCCACTTGCCAAACATT
TGACTCATTTTGTCTCCTCG	CTGAGTCTCGAACTTCTTCT	CAACCTTGGAATCCCATAGG	ATGGGCAGACATGCAGAACT
GGAAATGTTGACCCAGATTC	GTTGCTTTGAGGATTCTCCT	ATCCGACTTACTGTCAGGAC	TGGGAAGTCAAAGGTCTCCT
ACCTCCACACACATAACCAA	AACTGTCCAACGCATCCTTT	CGTTTCTTCCGAGATGGAGT	GGGTGAGGTTTTCTTCTCTG
GCCTGTTGCCCTGTTTTTAT	GATCCAAAGAGGCACCTTTA	TTTCCCATCCAGCCCACACA	ATTGACTTGTGTGGCCTCCA
TAGCTTGATCATCAAGGGTC	AAGTCCGGTCTCTAAACATG	GTGCACATTCGTTGCGGTAG	ATGGTAATACAGGCTCCACC
TCGAAGGACTGTAGACAACA	AAGTCGAGGGAATAGCTACA	ATCCACCACACAAGTGGAGC	TGAGGAGTGGTCATATAGGC
ACTTATTATGGCTCCTGGGA	TGTTCCATGGATTCCCCAAA	CTGTTCAGAAGAGGAGGGCT	TAAACTCAGCAGGGCCAAAG
TGTACCAAAAACGAGTGGCT	TCTAGTTCGTGTGAGATCAG	TTTTTTCCCGCCGCCACACT	GGCAACTAGCCTCTTTTCCA
ATTCCAGACTTGTACTGCTG	GCGCCGCGCTACATTTATTT	AGCTCATCGCAGAGAGAGCA	TAAATTCTGGGACATCCCGC
AAGCTGGGGTTGCAAATGAT	AACATCTTGGCCAGACGCTT	ATTGTCACTGGCACAGACCG	AATTCCGTCAGTCCCACACA
ATGTGGTAGGACACCAAACT	GGCGATTCTGAAACCAGGTT	TCCTTCATGGCACACTCGCT	
TCTGAAAAGGATTCCCCAGA	CTGTTCACTGGGCAAGTCTT	AGAAGCACGCCAGAAGAGCA	
AACAGAGGACATCATAGGCT	AAGTAGCCTTTATCCCCCTC	GGTCCTCCATGAACTGGCAG	
TGTCCTTTAGTGGGCCATTT	CGATGACTGTCATCCAGCAT	AGCCAGCAATTCCCAGCCTG	
TTGACCTCTTTATCCCCAAG	CCTTTTGTGCAGAGGTCGCT	AGCGGCCGTTCTTTGCTTGG	
ATTGTCAGCAGACTTGGTAC	AGAACCTCACTTGACCGCCT	TCGGTCCATGAGGTGCTCAG	
TTTGGAGAAAGGGTTCTCGA	CTCTCTCCCCCCGAATTTTC	ACAAGGGATGCAGTTGGGGG	
AAACCACAGAGGGGTTTGAT	TAACACCAGGGTCAGAGGCA	AACAGTCTGGGGCACAGACG	
AAAGGATTTCCGAAAGGGCT	GCGACCCAAGATGTCGTCGA	GGGCCCTTCCAGGTGATGTT	
TTCTTTGATGGCGCTTTCGG	TGTAGTCGTTCACCGTCCGC		
CCAACAAGTACTCGTCTGTC	AGGAAGGGGCTCCAGAGCAA		
TGCTTGTGTTGTCCCTGAGA	AGCTCGACGGTCTGGTCGTT		
GCTCTGTTGTCTGTCACATC	TCTCGGGTGGGGAGAGGTAT		
TAGGGCCTCACTTCCATTCT	CCCTGCTCACAGGAAGTGTC		
GTCTGAAGCAAGCAAGTCGT	CTCTGAGATCTCCGAGTCGG		
ATCCAGAAAGTTCGACTGCG	TGTCCACCTCCTGGTCGGAA		
CAGGAGCATTGCCTTTGAAG	TTGCCCCCACCTAAGTGCAC		
	ACAGACACCGGGAGCCAAGT		
	CTGTAGGGACTGCGTCATCC		